Environmental Challenges 15 (2024) 100906

Contents lists available at ScienceDirect

Environmental Challenges

journal homepage: www.elsevier.com/locate/envc

Enhancing water balance assessment in urban areas through high-resolution land cover mapping: Case study of Debrecen, Hungary

Douraied Guizani, Erika Buday-Bódi *, János Tamás, Attila Nagy

National Laboratory for Water Science and Water Safety, Institute of Water and Environmental Management, Faculty of Agricultural and Food Sciences and Environmental Management, University of Debrecen, 146B Böszörményi str., 4032 Debrecen, Hungary

ARTICLE INFO

Keywords:
Water balance calculation
Landsat 8
Landcover modelling
Remote sensing
Debrecen

ABSTRACT

Land cover (LC) mapping in urban areas is one of the core applications in remote sensing (RS), and it plays an important role in modern urban planning and management. In order to support up-to-date simplified water balance calculation, LC modelling needs to be developed for precise and high-resolution operations to monitor rapidly expanding urban areas. This study provides a spatial decision support tool for urban water balance calculations considering hydrological parameters at pixel scale. The study is aimed to create a high-resolution LC map for more precise water balance calculations to identify and link the most important parameters, such as crop coefficient, for estimating crop evapotranspiration, runoff coefficients, and infiltration rate. Meteorological data from 2016 to 2019 were involved in evapotranspiration estimation. The study site is Debrecen, a city in northeast Hungary with a population of about 200,000. By integrating Landsat 8 imagery, Google Earth (GE), and Corine Land Cover (CLC), a LC map of 30 m resolution was created with 81.2 % overall accuracy (OA) and a coefficient of kappa greater than 0.78. For the classification of Landsat 8, seven classes were assigned (forests, sealed surfaces, areas with crop cover, grassland, semi-sealed surfaces, bare ground and surface water bodies). Classification results were validated by 101 ground truth samples using other satellite images and aerial photographs. Water balance parameters (i.e. surface runoff, infiltration and evapotranspiration) were then defined and calculated at a pixel scale and for larger areas. The technique developed in this study can also be utilized in other urban areas.

Introduction

Water is one of the most vulnerable natural resources for drinking water, agriculture, industry, ecology, transportation, and economic activities (Duarte et al., 2015; Michelle et al., 2021). Although the Earth is called "the Blue Planet," growing population pressure, urbanization, economic development, and climate change are among the significant changes that greatly threaten the availability and quality of water resources (Frank and Benon, 2016; Srivastav et al., 2022).

An urban landscape has a significant impact on meteorological and hydrological dynamics (Qingyan et al., 2021). Urbanization in a watershed can create substantial changes to urban microclimate affecting the natural water cycle of a city. Meanwhile, LC changes affect the whole water cycle. The increase of impervious surfaces due to the construction of roads or roofs increases runoff, decreasing infiltration and evapotranspiration (Dams et al., 2013; Weng and Lu, 2008). Ramier et al. (2011) studied the effects of impervious surfaces on two streets in Nantes (France) over 38 months, demonstrating the increase in runoff with urbanization in their study area. Consequently, it is also linked to the organization of hydrographic networks (natural or entropized) (Vrebos et al., 2014), which can also increase the risk of flash floods or extreme urban microclimates, like increased urban heat island effect (Manandhar et al., 2023). Al Kafy (2022) explores the impacts of urban expansion on surface urban heat island intensity using neural network algorithms, which highlight the potential application of similar modelling approaches to assess the impact of LC changes on the water cycle in rapidly developing urban areas. On the one hand, summer precipitation is influenced by thermodynamic effects contributing to changes in the structure and instability of clouds (Moradi et al., 2022). On the other hand, the marginal presence and loss of vegetation in urban areas combined with increased soil sealing initiates a decrease in evapotranspiration, which explains the lower relative humidity in urban areas compared to the neighbouring rural areas resulting in the urban heat island effect (Rahman et al., 2022). These findings demonstrate how

* Corresponding author.
E-mail address: bodi.erika@agr.unideb.hu (E. Buday-Bódi).

https://doi.org/10.1016/j.envc.2024.100906
Received 7 December 2023; Received in revised form 19 March 2024; Accepted 28 March 2024
Available online 2 April 2024

crucial it is to examine the links between LC changes, the effects of urban heat islands, and the water cycle in rapidly growing urban areas. For effective management of water sources in urban systems, precise tools and quasi-real-time data are required to calculate the water balance of urban sites automatically. Nieuwenhuis et al. (2021) emphasize the gap between available meteorological, hydrological, LC, and soil data and their utilization in an integrated urban water management system. Out of several studies, the following researchers are dealing with hydrological data assimilation challenges and offering possible solutions to ensure proper inputs for modelling. Son and Kwon (2022) recommend the calculation of infiltration and runoff specifically for urban parks based on field experiments to acquire high accuracy, while other studies focus on implementing fewer parameters into analysis but with a high temporal resolution for long-term simulation (Thorndahl et al., 2019; Yang et al., 2022).

LC is one of the most important temporarily changing data in hydrological modelling influenced by human activities (Chemak et al., 2022). LC data such as CLC and Urban Atlas are available for Europe with a spatial resolution of 100 m and 10 m, respectively (European Environment Agency, 2023). From a temporal perspective, these datasets provide information only every sixth year, in the former case since 2000, while in the case of Urban Atlas since 2006, which is questionably sufficient information to express LC characteristics of the continuously changing urban regions (Njoku and Tenenbaum, 2022; Lia et al., 2022). Therefore, there is a need for improved LC modelling and water balance calculations in rapidly developing urban areas. Al Kafy (2023), emphasize the relevance of machine learning algorithms in analyzing water related vulnerabilities in urban areas by presenting a method for assessing and predicting agricultural drought vulnerability using machine learning. One of the most effective techniques for efficiently retrieving data on LC is remotely sensed (RS) image classification (Jensen, 2000). The classification process enables the identification and extraction of features from objects of interest or phenomena (Shi and Yang, 2015). Classification of RS images has been the focus of numerous studies (Rong et al., 2023; Naboureh et al., 2020), the variety of data sets and classification methods still makes this as a challenging task (Mehmood et al., 2022; Boulila et al., 2021). The RS image classification process is usually divided into a few key sections, comprising deciding a suitable classification technique, pre-processing the data, collecting training samples, extraction of features, post-classification processing, and accuracy assessment (Schott, 2002). The analyst's knowledge of the geographic area under consideration and its LC is essential for training the algorithm (Jensen, 2000). However, collecting ground truth details is a time-consuming and expensive task (Bruzzone and Prietro, 2001). The precisely calculated information on LC categories' hydrological properties (e.g., runoff, infiltration) are also limited (Kim et al., 2022). Guha et al. (2022) demonstrated the use of regression and geospatial methods to predict solid waste generation rates and identify optimal landfill locations. This approach can be integrated with RS data and hydrological parameters to enhance urban water modelling efforts. Using GE and the InVEST model, Al Kafy (2023) integrated dynamics of carbon storage and changes in forest cover, highlighting the significance of integrating modelling and RS methods to study changes in LC and their effects on the water cycle.

Since 1990, a significant increase in the extent of artificial surfaces, particularly in urban catchment areas, has been seen in Eastern European countries, including Hungary (Hardi et al., 2020; Cieślak et al., 2020). Also, the application of LC databases (including CLC) and statistical analyzes to investigate urban and industrial sprawl pattern are quite rare in Hungary, with a few exceptional examples like Szilassi (2017) and Kovács (2011) which do not focus on urbanization patterns. Furthermore, the motivation for compact urban planning was missing from the regulatory environment until 2019 and country-level studies primarily examined the Budapest (the capital of Hungary) agglomeration (Lennert et al., 2020; Kovács et al., 2019).

This study aims to develop a RS-based and geographical information system-based (GIS-based) spatial tool for LC classification method and mapping to foster more accurate water balance modelling urban sites. The main goal of this study was to develop a quick and quasi-real-time LC mapping method for the rapidly developing urban regions using the classical Maximum Likelihood Classifier (MLC). Within this study, authors aim to develop a Landsat 8 based, flexible, high resolution (30 m) LC classification method which integrates hydrological, meteorological, and geographical data to improve the urban water balance calculations. Implying complex data collection and processing, the use of LC classification method for the study area and hydrological coefficient calculations for each LC categories shall contribute to estimate the hydrological cycle parameters at pixel scale and to define urban water balance to larger scale for each LC category. Generating up-to-date water balance parameters and proposing a framework can provide a valuable tool for tracking LC changes and their influence on the water cycle dynamics in rapidly changing urbanized regions.

Materials and methods

Description of the study area

Debrecen is Hungary's second-largest city. It has a total area of 461.25 km^2 and a population of around 203,000–207,000 people. Optimistic urban development plans predict that, by 2050, there will be a population growth of 30,000–50,000 (STRATEGY 24). Debrecen is the regional capital of the Northern Great Plains region and is situated near the eastern border of the European Union (Fig. 1a).

Debrecen is a middle-sized city, the cultural, administrative, educational, and commercial centre of eastern Hungary (Tamás et al., 2019; Kozma and Molnár, 2021). Debrecen's economy is developing dynamically nowadays (Molnár et al., 2018). In the last five years, more than 1200 hectares of new industrial land have been designated in Debrecen (North Western Economic Belt, Southern Industrial Park), where further development of the infrastructure is proceeding rapidly (Molnár and Kozma, 2018). The LC of dozens of hectares is foreseen to change in the following years. Debrecen has the largest developing office capacity in Hungary after the capital, which continuously expands. Similarly, the industrial parks of the city show growth in both area size and diversity (Kozma and Molnár, 2018), resulting in rapidly developing. Debrecen's green space system is characterisized by the duality of the city's landscape and environment: in the northeast and east, there are significant forest areas, while in the west, there are areas of intensive agriculture. A considerable part of the forested areas is located on the northern outskirts. Over the last few decades, Debrecen has seen a significant increase in suburban, periurban residents, resulting in the city's dispersion (Pénzes et al., 2023). These processes also contribute to the rapid changes in the hydrology of Debrecen. Moreover, noteworthy modifications have been started including substantial LC changes due to intensive industrial investments since 2019, affecting several parts of the city (Iváncsics and Kovács, 2021). Many of these changes involve large water and labour-intensive automotive and battery industry facilities that have a significant impact on employment, leading to population growth. Due to these significant LC and resource demand changes which have been still in progress, we targeted to define the temporal frame of this study between 2016 and 2019 when the changes in LC were dominant.

Debrecen shows a duality in terms of water resources. While surface water resources are inadequate, the region is rich in groundwater, attributable to geological and geomorphological factors. Several studies have been conducted to access the hydrological characterization of Debrecen (Tamás et al., 2019; Brodmann, 2016). Geological investigations of Urbancsek (1960) and Borsy (1989) indicate that during the Pleistocene period, the Tisza River and its tributaries shifted northward and shaping the current landscape. Descriptive and geomorphological analyzes, including Lóczy's studies (1997) and subsequent works by Lóczy et al. (2009), revealed that the development of

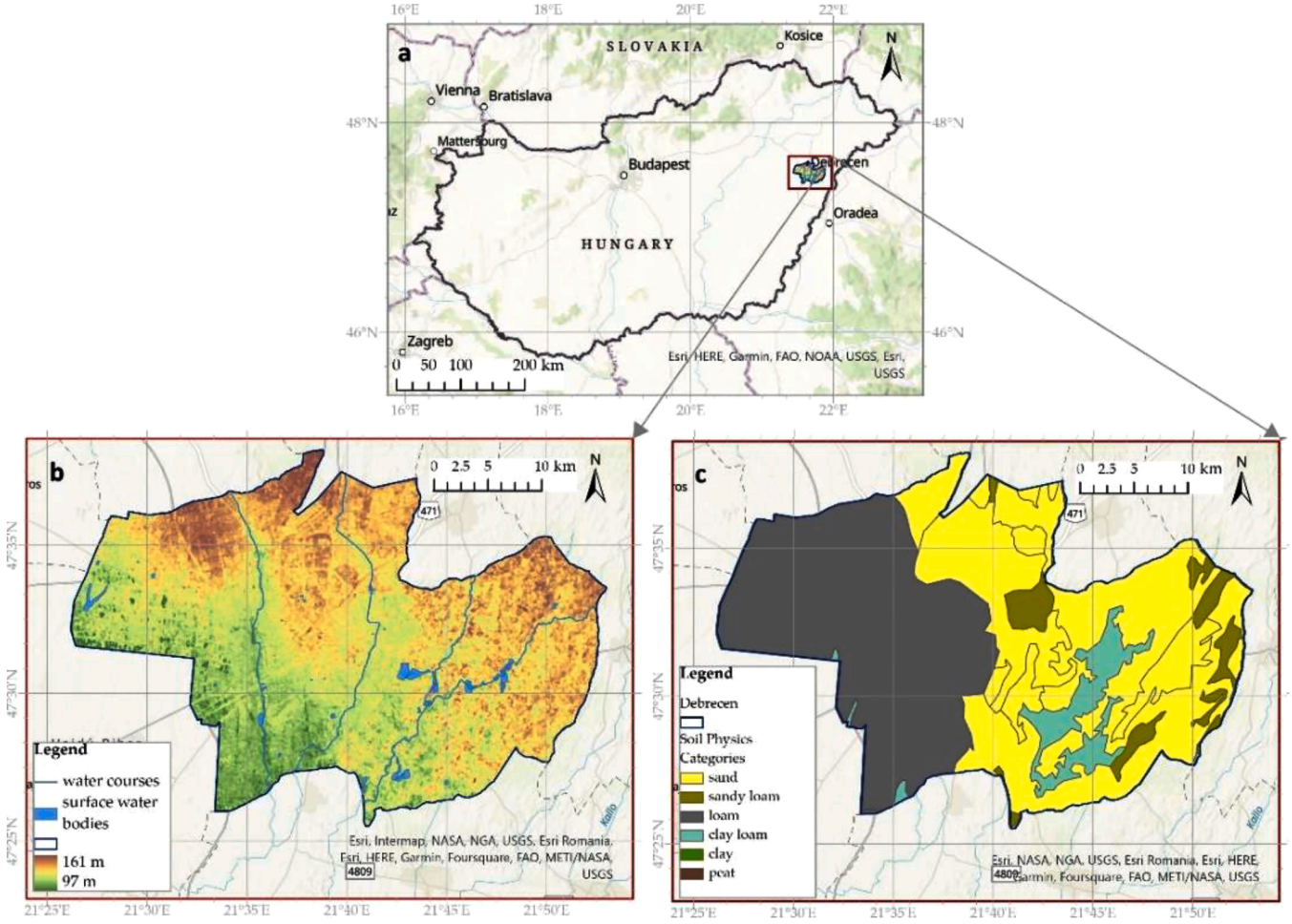

Fig. 1. Location of study area (a), digital elevation model and hydrographic network (b), and soil physical categories of Debrecen (c).

smaller, lower-yield watercourses due to this northward migration, resulted in diminished water inflow to the region. Presently, on the city's west side, several similar ephemeral stream water resources can be found with low discharge, such as the Tócó Creek. On the east side, the Kondoros Creek, which is also characterized by low discharge, flows towards the Berettyó and Hortobágy rivers (Fig. 1b). Low discharge and high environmental impacts and pressures result in poor water quality. The reduced inflow of fresh water makes the ecosystems more vulnerable, presenting both qualitative and quantitative threats, as noted by Somlyai et al. (2019). In response to these challenges, various systems (aquatic and water-related terrestrial ecology, technical-hydrological, meteorological) undergo assessments, monitoring, and propose interventions to help decision-makers and stakeholders in a meaningful way (Hüse et al., 2016; Pregun, 2022). The hydrographic network represents all the watercourses (creeks, lakes) (Tony and Jorge, 2022), and in the case of Debrecen, they must be utilized and maintained with great caution, while the groundwater resources are also essential mainly due to drinking water supply, energy production and balneological purposes. It is also a great challenge to assess the environmental impacts of all members of the hydrological system of Debrecen (Buday-Bódi et al., 2019).

The city is situated on a small landscape characterized by an alluvial fan plain, a flat area in the neighbourhood is covered by a thin layer of shifting sand. On the east, particular types of parabolic dunes develop beyond the Kondoros watercourse. The north-northeast to south-southwest oriented valleys divide this area horizontally and provide unique morphological characteristics. Based on the ASTER database (ASTER Science Team (2013)), the highest altitude is around 161 m in Debrecen, and the lowest is approximately 97 m (Fig. 1b). Fig. 1(c) illustrates the distribution of soil texture classes based on the Hungarian agro-topographic map (AGROTOPO) (Bakacsi et al., 2014). There are six primary soil texture groups: sand, sandy loam, loam, clay loam, clay, and peat. The most common groups are sand and loam, followed by sandy loam, clay loam, clay, and peat.

Based on a 29-year meteorological dataset from 1991 to 2020, the hottest years occurred after the turn of the millennium and during the final decade of the previous century, the two hottest years were successively 2011 and 2012 (Szalai et al., 2005). According to Debrecen's long-term average monthly temperatures (1991–2020), January is the coldest month and August is the warmest. The average annual temperature fluctuation is 22.7 °C (Fig. 2a). Debrecen has a humid continental climate with rainfall even in the driest months. The most variable climate element in this region is precipitation. Between 1991 and 2020, the average annual rainfall is 546 mm. The least amount of precipitation falls between January and March, while the highest precipitation, more than twice as much, occurs in May-July (Fig. 2a). The annual amount of global radiation was 4631 MJ/m^2 between 2001 and 2020 with a maximum in June-July (the monthly amount surpasses 680 MJ/m^2 in July) and a minimum in December-January (the monthly amount is on average 100 MJ/m^2) (Fig. 2b). Debrecen has an average annual wind speed of 3.02 m/s. Wind speed distribution throughout the year is characterized by a spring maximum, with the March average being 3.72 m/s, and the lowest recorded value being in August (2.61 m/s) (Fig. 2c). The most frequent wind direction is northeast; in 21 % of the cases, the wind blows from the prevailing wind direction, while the south direction has the second highest relative frequency (18 %). Most rarely, the wind

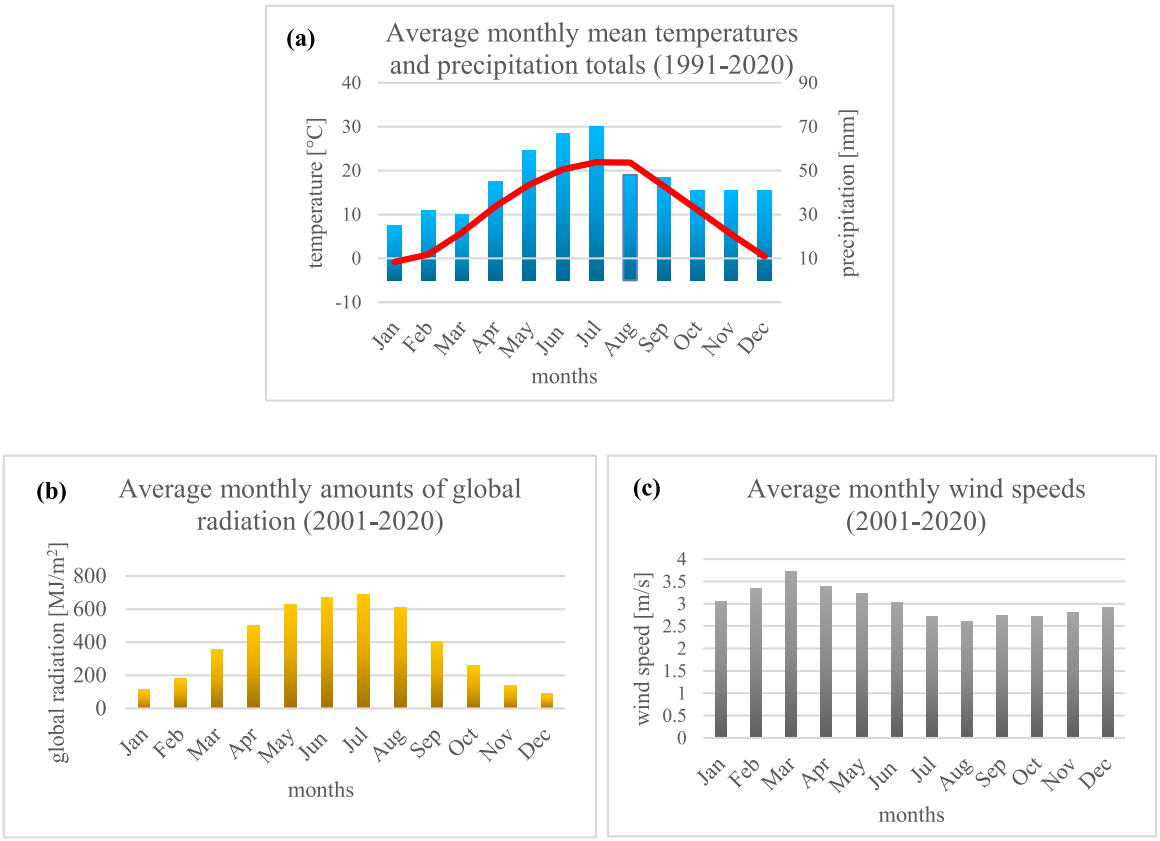

Fig. 2. Climatic characteristics of Debrecen: Average monthly mean temperatures and precipitation totals (1991–2020) (a), Average monthly amounts of global radiation (2001–2020) (b) and Average monthly wind speeds (2001–2020) (c).

blows from the northwest (Szász et al., 2013). Daily data for minimum temperature, maximum temperature, mean temperature, solar radiation, relative humidity, wind speed, and sunshine hours were obtained from the open access meteorological database Power Data Access Viewer (https://power.larc.nasa.gov/data-access-viewer/).

Overall framework of the study

The first goal of this study was to create a small-scale LC map based on Landsat 8 satellite data and to identify and link the most important parameters for more precise water balance calculations. Our analysis relied on a robust data collection and processing workflow. We established a geodatabase to organize various data sources, including satellite imagery, climate records, and digital elevation models. GIS were then employed to analyze the spatial relationships between these datasets. Digital Terrain Analysis provided insights into the land's topography, crucial for understanding hydrological parameters. Satellite image processing enhanced the imagery, allowing for accurate LC classification

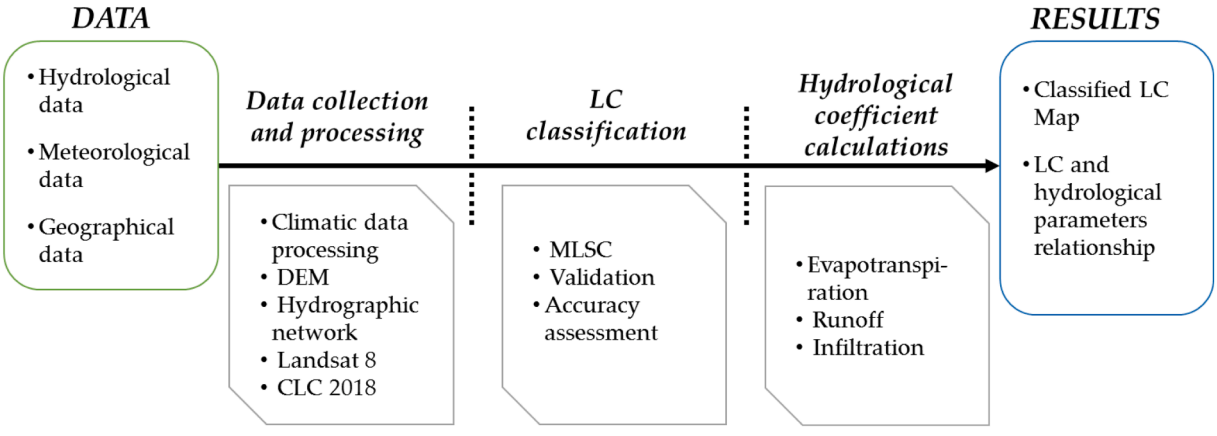

DEM: Digital Elevation Model
CLC: Corine Land Cover
LC: Land cover
MLSC: Maximum Likelihood Supervised Classification
UWB: Urban Water Balance

Fig. 3. Scheme of Urban Water Balance (UWB) analysis.

(Sajikumar and Remya, 2015). Finally, climate data processing enabled us to study how climatic factors influence these hydrological parameters. These parameters included crop coefficient for estimating crop evapotranspiration (ET_c) and runoff coefficient to calculate infiltration rate for the LC categories. For ET_c estimation, meteorological data for the reference period of 2013–2019 was used. The research consists of three steps (Fig. 3).

Spatiotemporal data acquisition

Landsat 8 and internationally available LC (e.g. Urban Atlas, CLC) RS data time series images were processed and integrated to calculate the water balance of the city. The study employed Landsat 8 data, which is freely available and has a high spatial resolution of 30 metres (Nwagoum et al., 2023). Data from Landsat 8 (30 m resolution) from 2013 to 2019 have been freely downloaded from U.S. Geological Survey (USGS) website (USGS, 2016). The Worldwide Reference System (WRS) ID for the downloaded scenes path/row was 186/27, with cloud cover range between 0 % and 35 % (Table 1). Each Landsat 8 Collection 1 Level-1 image consists of 11 electromagnetic spectrum bands. Landsat 8 is using nine Operational Land Imager (OLI) 0.45 - 1.38 μm and two Thermal Infrared Sensor (TIRS) bands 10.60 - 12.51. Landsat 8 is one of several sensors used for LC classification, alongside Moderate Resolution Imaging Spectroradiometer (MODIS) and Sentinel 2. MODIS, a low spatial resolution sensor (500 m), provides global coverage (Xu et al., 2024), while Sentinel-2, a high spatial resolution sensor (10 m), offers regional coverage (Acharki, 2022). Compared to high-resolution sensors, low-resolution satellite images have a much better synoptic view and temporal revisit frequency system because of their large swath width. However, the accuracy of yield detection, the interpretation and validation of the signal, and the reliability of the derived information products have usually been complicated because of insufficient spatial resolution and sub-pixel signal mixture (Rembold et al., 2013). Furthermore Landsat 8 generally surpasses MODIS for LC classification due to its higher spectral resolution, enabling better spectral separability between LC classes. However, MODIS remains valuable for LC monitoring due to its higher temporal resolution (daily acquisitions compared to Landsat 8's 16-day repeat cycle) (Klein et al., 2012). The higher the spatial resolution of RS data is, the better its assistance will be in identifying small objects. Although Landsat (or similar sensors, such as Satellite Pour Observation de la Terre (SPOT)) is also the primary data source, with sufficient spatial resolution in most agricultural, urban, periurban, suburban, and rural areas, and a 16-day gap between successive images, obtaining cloudless images in Hungary during the growing season in humid years can be difficult (Lobell, 2013). Additionally, Landsat 8 maintains a longer data acquisition history compared to Sentinel-2 and MODIS. This extended time series provides valuable insights for tracking long-term LC changes (Roy et al., 2014). Before classification, required data were pre-processed using layer stacking. Urban Atlas, a GIS database produced by the European Environmental Agency, is widely used by researchers due to its open access status and high quality (European Environment Agency, 2023). Urban Atlas provides statistical and spatial information for 800 European Functional Urban Areas, including LC categories, population, and spatial data for various LC patches (Poleman, 2018; Barranco et al., 2014). Urban Atlas and CLC database were used in this research, especially to differentiate between sealed and semi-sealed metropolitan areas.

Table 1
List of Landsat 8 datasets used in this study.

Season	Landsat 8 Product Identifier L1	Acquisition time
2013 Summer	LC08_L1TP_186027_20130809_20200912_02_T1	2013-08-09 09:22
2013 Winter	LC08_L1TP_186027_20140116_20200912_02_T1	2014-01-16 09:21
2014 Summer	LC08_L1TP_186027_20140609_20200911_02_T1	2014-06-09 09:20
2014 Winter	LC08_L1TP_186027_20150220_20200909_02_T1	2015-02-20 09:20
2015 Winter	LC08_L1TP_186027_20150220_20200909_02_T1	2015-02-20 09:20
2015 Summer	LC08_L1TP_186027_20150612_20200909_02_T1	2015-06-12 09:19
2015 Summer	LC08_L1TP_186027_20150815_20200908_02_T1	2015-08-15 09:20
2016 Winter	LC08_L1TP_186027_20160207_20200907_02_T1	2016-02-07 09:20
2016 Summer	LC08_L1TP_186027_20160630_20200906_02_T1	2016-06-30 09:20
2017 Winter	LC08_L1TP_186027_20170225_20200905_02_T1	2017-02-25 09:20
2017 Summer	LC08_L1TP_186027_20170804_20200903_02_T1	2017-08-04 09:20
2018 Winter	LC08_L1TP_186027_20171226_20200902_02_T1	2017-12-26 09:20
2018 Summer	LC08_L1TP_186027_20180807_20200831_02_T1	2018-08-07 09:19
2019 Winter	LC08_L1TP_186027_20190215_20200829_02_T1	2019-02-15 09:20
2019 Summer	LC08_L1TP_186027_20190607_20200828_02_T1	2019-06-19 09:20

Methods

LC classification

Fig. 4 summarizes the comprehensive workflow, showcasing the multiple stages of data processing, calibrations, and validation implemented to produce the classified image effectively.

Selection of algorithm and classification. MLSC (Ali et al., 2018) was used to classify Landsat 8 satellite images to obtain a LC map with 30 m spatial resolution. The ML decision rule is the most popular supervised classification approach for evaluating satellite image data (Medina and Beatriz, 2018). Several researchers used supervised classification for LC extraction (Ahmad and Quegan, 2012; Asuquo et al., 2023). Methods that provide supervised classifications enable a prompt and typically outstanding result (Weng and Lu, 2008). MLSC cannot handle complex images. Thus, a high number of pixels cannot be classified correctly (Blaschke, 2010). The selection of initial values can significantly impact the performance of MLSC, introducing potential biases and estimation errors. Additionally, MLSC may not exhibit optimal properties when dealing with small sample sizes, despite these limitations, MLSC is often employed for images characterized by low spatial resolution (Mustapha et al., 2010). On the other hand, Bolstad and Lillesand (1991), highlighted MLSC's effectiveness in handling scenarios with normally distributed data, its ability to produce reliable results despite such challenges and can run in limited memory desktop computer environments. Through a comprehensive review of LC classification methods from 1984 to 2019, Daba and You (2022) highlighted the ML algorithm as a powerful and versatile tool for LC classification. Its accuracy, robustness, and sensitivity to spectral variability make it suitable for various applications, including urban planning, environmental monitoring, and LC change detection over time (Daba and You, 2022).

Supervised classification methods require consistent pre-classification input from the image analyst. For the urban area, the CLC database was used to collect training points on the sealed and semi-sealed parts of Debrecen. Pre-processing of the Landsat 8 data involved selecting training points for LC classification and generating Normalized Difference Vegetation Index (NDVI) (Tucker, 1979) and composite images to enhance spectral information for LC mapping. NDVI derived from Landsat 8 in delineating of vegetation-covered area. Consequently, various Landsat composites were used to gather training points across various LC types in Debrecen, including agricultural areas with crop cover, bare ground, pastures, and forest regions (Qin et al., 2021). In total, 210 training samples were assigned to seven LC classes as training

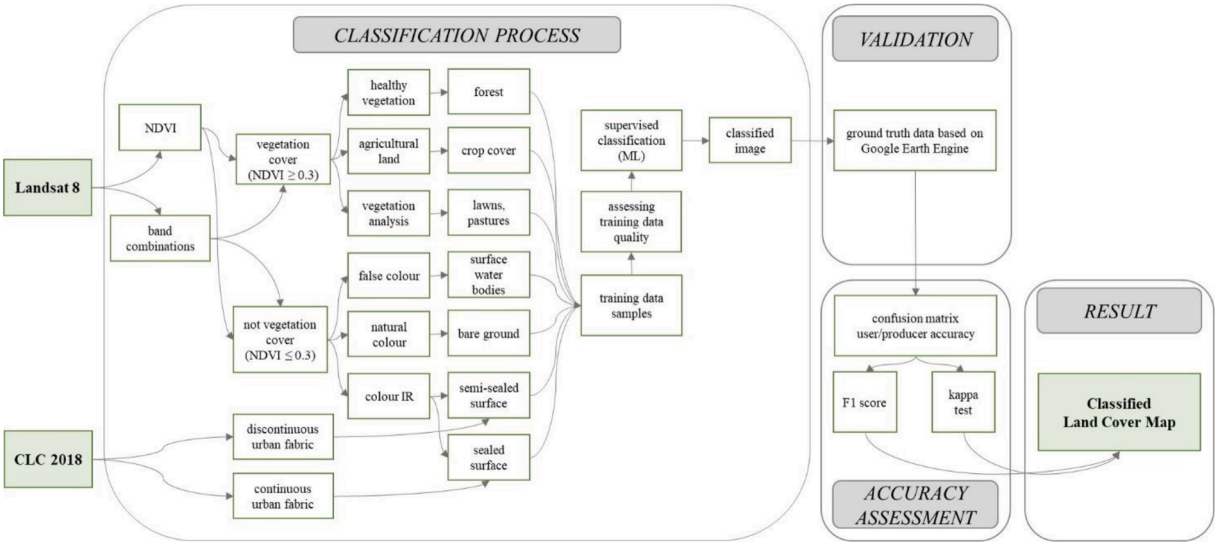

Fig. 4. Schematic representation of the data processing workflow for image classification.

points, with 30 training Regions of Interest (ROI) units in each category, selected and edited as pixels on each evaluated band combination of Landsat 8 images (Dou et al., 2024). All these pixels fulfil the requirement of representativeness of the selected category.

Drawing from the findings of Jamshid et al. (2013), seven composite datasets from Landsat 8 were employed to choose training points for various LC categories. Based on field survey in the study area, seven categories were defined (Table 2).

This approach leverages the unique sensitivity of different band combinations to particular LC categories, as detailed in Table 3. Various composites facilitated the selection of different training sites, serving as a vital step in the classification process.

The higher the number of the samples provided for the classification as training points is, the more accurate the final obtained LC map can be (Zhu et al., 2016; Zhou et al., 2022).To improve accuracy and reduce complexity, NDVI were derived from Landsat 8 data. NDVI was used for vegetation masking using 0.3 as a threshold for vegetation cover. Pixels with NDVI values higher than 0.3 were considered vegetation (Lemenkova, 2018). This NDVI mask was used with the composites to collect the training points for vegetation covered sites. In this LC classification study, 30 training points per class were selected manually and randomly. Finally, 210 training points were compiled and distributed across seven specific LC categories. Before the selection of these training points, the data underwent the following pre-processing steps:

Table 2
LC categories defined based on field surveys and their definitions.

Category	Definition
Sealed surfaces	artificially covered surfaces, buildings, and roads, typically covering more than 80 % of the area of the identified spatial unit (Linda and Geir, 2021)
Areas with crop cover	relatively homogeneous, thus easily identified in the Landsat data due to their spectral characteristics and regular field geometry (Matthews et al., 2022)
Grassland and pasture ground	covered with herbage or grass, dominated by grass or grass-like vegetation, used or suitable for livestock grazing (Schoenbaum et al., 2018)
Semi-sealed surfaces	buildings, roads, and artificially covered surfaces covering between 50 % and 80 % of the total area of the unit (Linda and Geir, 2021)
Forests	forests are land occupying an area of more than 0.5 hectares with trees reaching a height of more than 5 metres and a canopy cover exceeding 10 % (FAO, 2000)
Bare ground surfaces	includes the soil or sand not covered by grass, sod, other living ground covers, gravel, wood chips, artificial turf, or similar covering (Liu et al., 2022)
Surface water bodies (SWB)	reservoirs, ponds, lakes, or inland excess water with open water surface (Williams et al., 2004; Monaghan et al., 2017)

Table 3
Band combinations of Landsat 8 used for training point selection across LC categories (Jamshid et al., 2013).

Name of composite	Spectral band combination (RGB)	Role in the training site collection
Natural Colour	4 3 2	Bare ground
False Colour	7 6 4	Urban area/Water
Colour Infrared	5 4 3	Urban area/Vegetation
Agriculture	6 5 2	Agriculture
Healthy Vegetation	5 6 2	Forest
Vegetation Analysis	6 5 4	Vegetation

1. SWB´s and bare land were separated, utilizing a 7–6–4 band composition, which respectively appeared as very dark blue and yellowish in the imagery. Subsequently, training points for water-covered areas (30 training samples) were chosen and labelled as water bodies.
2. Distinguished by their rectangular shape and geographical location, areas with crop cover were differentiated from other elements. Vegetation was identified using the 6–5–2 band composition, which facilitated the distinction between dark green, associated with forest areas, and light green, representative of areas with crop cover. NDVI, a notable spectral index, was utilized to emphasize the differences in LC between vegetation-covered and non-covered areas. Consequently, high NDVI values (0.6–0.8) were observed, aligning with the expected characteristics of the forest category.
3. The colour infrared band composition (5–4–3) was utilized for sealed and semi-sealed locations, effectively identifying urban areas that appear as light blue. Urban areas, characterized by low NDVI values, ranging from 0.2 to 0.5, were thus discernible. In addition, since the delineation of these two urban types from each other is not possible solely by Landsat 8, the CLC 2018 data were applied. Finally, the selected training points (30 points) were merged under the name of the sealed surface category.
4. The bare ground land type classification leverages two distinct band compositions, 6–5–4 and 5–6–2, wherein bare land exhibits a brown hue. Both these composites and the NDVI layers were reclassified to

represent soil. In terms of the composites, any pixels bearing a brown colour were classified as bare ground. Meanwhile, for the NDVI layer, pixels with values ranging between 0 and 0.2 were categorized as bare ground. These layers were subsequently intersected, yielding pixels with a heightened likelihood of representing the bare ground.
5. The calibration points for lawns and pasture were selected based on CLC 2018 data.

Validation of classification. After completing the training point selection, the samples were consolidated, and each class was appropriately labelled. The subsequent mapping and statistical evaluation tasks were executed utilizing Environment for Visualizing Images (Envi v5.3) (Bruse and Fleer, 1998). The proceeding phase involved the systematic calculation of spectral separability, a method known for its precision in verifying the selection of training points. Separability indices, such as the Jeffries-Matusita (J-M) and the Transformed Divergence distance (TD) (Padma and Sanjeevi, 2014), express values ranging from 0 to 2, where 0 signifies complete overlap and 2 denotes perfect separability. To have more accurate and up-to-date data for better computation of water balance parameters, the resulting LC map was calculated for the specific year of 2019.

Accuracy assessment of classification. To determine the quality of the classification results, the most widely used measures (overall, producer's, user's accuracy, and kappa coefficient) were derived from Confusion Matrices (CM) (Lunetta et al., 1991). Verifying RS-based data is one of the prerequisites for adequately utilizing and understanding the data (Nagy et al., 2007, 2009, 2013). Conducting an accuracy assessment is a critical component of any classification project. This process involves comparing the classified raster image with an established, reliable validation data source, such as GE and CLC images (Yonaba et al., 2021). The sampling frame was defined as the area of available very high spatial resolution imagery. Sample units were defined as 30×30 m pixels. Using a stratified random sampling approach, validation sample units proportional to the area of each LC stratum within the sampling frame were selected, increasing sampling intensity for less common classes (Hermosilla et al., 2018). The results were validated by other satellite images and aerial photographs (GE and CLC 2018) at high spatial resolution, up to 10 m and 100 m, respectively (Liu et al., 2020). 110 random points per category were generated using validation data from GE and the Urban Atlas. Notably, the Urban Atlas proved invaluable for collecting validation points, confirming the differentiation between sealed and semi-sealed LC categories.

To address concerns regarding spatial autocorrelation, a minimum distance between the nearest samples units of ≥500 m was established (Su et al., 2020). In total, 770 validation points were selected and distributed among the classes. The accuracy of the newly classified LC map was assessed by comparing these sampling points with the classified data within a confusion matrix. The Kappa index (Cohen et al., 1960), used in this study is one of the most widely applied method and constitutes the core of the accuracy assessment in several previous studies (Foody, 2006; Foody 2020; Li et al., 2022). On the other hand, there is growing body for using overall, producer's, user's accuracy measures as allocation and quantity disagreements instead of Kappa for a more comprehensive assessment (Bayraktar et al., 2024). This shift stems from limitations of the kappa index in considering randomness in a misleading baseline (Pontius and Millones, 2011; Pontius, 2022), and its accuracy in reflecting true agreement is debated (Feizizadeh et al., 2022). Furthermore the challenges of interpretation due to prevalence and bias (Foody, 2020), has led to avoid kappa-based index for general map comparisons (Pontius and Millones, 2008). Therefore, to provide a more detailed assessment, we evaluated accuracy within individual categories using producer's and user's accuracy. Producer's accuracy focuses on errors of omission (Naesset, 1996), while user's accuracy considers errors of commission (Rosenfield and Fitzpatrick, 1986). Moreover, OA was used in our study to assess the general agreement between the reference and simulated map (Varga et al., 2019). Additionally, the F1 score was computed. The F1 function returns the F1 score, representing the harmonic mean of the user's and producer's accuracy values (Yonaba et al., 2021).

Hydrological coefficient calculations

Hydrological coefficient calculations for defining urban water balance aimed to estimate the hydrological cycle parameters at pixel and larger scale for each LC category. To simulate the flow and transport of surface water and groundwater, several physically based distributed models, including Soil & Water Assessment Tool (SWAT) (Mtibaa and Asano, 2022), Water and Energy Transfer between Soil, Plants and Atmosphere (WetSpa) (Safari et al., 2012), and MIKE SHE Integrated Hydrological Modelling System (Sandu and Virsta, 2015), are available. This study focuses on the simplified calculation of water balance parameters using the runoff coefficient, applying local references determined for Eastern Europe, and estimating evapotranspiration through the use of the empirical Turc formula (Turc, 1961). The rate of infiltration at a particular LC type was determined using the Turc equation, chosen for its advantage of requiring a limited amount of meteorological parameters (temperature and precipitation) (Diouf et al., 2016). Initially, the mean annual temperature and precipitation were calculated for 2016–2019 to derive the evapotranspiration coefficient for different LC categories within the watershed.

Evapotranspiration. Due to the significant standard deviation observed over the 4 years, relying solely on the average annual precipitation was deemed inadequate to represent the mean value accurately. Therefore, the 'centre' P_{MM} value of the precipitation range within the basin was determined. The Eq. (1), is a method for calculating the median of a set of precipitation values. The median is the middle value in a sorted distribution, and it can be used to represent the "central" precipitation value for a given region or time period. This formula is commonly used in hydrology and climate science studies to analyze precipitation data (Soil and Water Conservation Society, 2003). It is a simple and straightforward method that can be applied to both historical and real-time precipitation data sets.

$$P_{MM} = \frac{P_{min} + P_{max}}{2} \tag{1}$$

Where,

P_{MM} represents the mean annual precipitation [mm/year],
P_{min} is the minimum mean value of precipitation [mm],
P_{max} is the maximum mean value of precipitation [mm].

Based on the climatic data utilized in this study, the minimum mean annual temperature (T_{min}) was 11.1 °C, while the maximum mean annual temperature (T_{max}) reached 12.5 °C. Similarly, the minimum mean annual precipitation (P_{min}) was recorded at 435.9 mm, while the maximum mean annual rainfall (P_{max}) measured 743.9 mm. The 'central' mean annual precipitation of the basin (P_{MM}) was determined to be P_{MM} = 589.9 mm. By integrating the Turc formula with P_{MM}, T_{min} and T_{max}, the minimum and maximum values for the average annual reference evapotranspiration within the basin were derived.

The mean annual evapotranspiration was determined using the Turc formula (Turc, 1961; Osorio et al., 2014; UNESCO OMM AISH, 1974) (Eq. (2)).

$$E = \frac{PMM}{\sqrt{0.9 + \frac{PMM^2}{\left(200 + 25T_{mean} + 0.05T_{mean}{}^3\right)^2}}} \tag{2}$$

Where,

E represents the reference evapotranspiration [mm/year],
P is the annual amount of precipitation [mm/year],
T_{mean} is annual mean temperature [°C].

Tallis et al. (2013) conducted an extensive literature survey and generated their own set of crop coefficient (K_c) values utilized in this study (Table 4). Understanding the phenology and growth stages of the vegetation is necessary for utilizing these coefficients. Additionally, this literature survey and manual suggests that evapotranspiration coefficients can be applied to the non-vegetated class, encompassing bare ground or water bodies. Impervious surfaces, in general, are assigned a very low value (such as 0.001) for the K_c coefficient, highlighting their minimal influence on the overall drainage process. In contrast, stagnant or slow-flowing water is assigned a coefficient close to 1, as Tallis et al. (2013) defined.

In this study, we have calculated evapotranspiration coefficients for each LC class in Debrecen based on the specific vegetation types within each class. To achieve this, a crop coefficient (K_{cn}) must be defined for each LC class for Debrecen. In this context, the following approach was employed: First, the determination was carried out for homogeneous classes as presented in Tallis et al. (2013). Then, the average K_c value for each LC was calculated based on its respective area (Table 4). As an example, for the "Sealed surface" class, the values of the "urban" and "built" type crop coefficients were used. For the "Semi-sealed" category, the average of 4 class types, namely urban, bare ground, wooded meadow, and open shrubland were used.

This study calculated the reference evapotranspiration (ET_0) on watershed scale, representing the overall evapotranspiration value for all LC classes combined. Eq. (3) (Kashyap and Panda, 2001) outlines evapotranspiration calculation for each specific LC class (ET_{cn}) within the Debrecen basin.

$$ET_{cn} = K_{cn} ET_0 \tag{3}$$

Where,

ET_{cn} maximum annual evapotranspiration for each LC class [mm],

n represents the number of the LC class ($n = 1, 2, 3, 4, 5, 6, 7$),

K_{cn} is the crop coefficient for the n^{th} LC class,

ET_0 is the mean annual reference evapotranspiration in a watershed [mm].

Runoff. The Kenessey (1928, 1930) equations and coefficients, validated, adopted, and widely used in Eastern European conditions (Hungary, Romania, Slovakia, and Ukraine), were employed to calculate the runoff ratio. This approach is specifically tailored to the morphological context of Eastern Europe. The method involves determining the watershed's runoff coefficient (or flow factor) by summing partial coefficients that account for factors such as slope steepness, soil and bedrock permeability, and vegetation cover. Kenessey (1928, 1930) introduced a table that includes the average runoff coefficients for Hungary, incorporating various factors. These factors consist of slope conditions and their associated factors α_1, permeability conditions with factors related to soils and surfaces α_2, and sterility conditions along with factors α_3 that pertain to vegetation cover (Table 5). The overall runoff can be determined by summing the contributions of α_1, α_2, and α_3.

The runoff coefficient for each LC category was determined using Kenessey coefficients. The landscape for our site is mainly flat, regarded as gentle slope with a value less than 3.5 %. The Hungarian agro-topographic map (Várallyay and Molnár, 1989) was utilized to determine the soil textures within the study area (Fig. 1c). This map is a nationwide soil geoinformation system initially compiled and presented on topographic map sheets on a scale of 1:100 000. Approximately 3 500 soil mapping units (SMU) are represented as polygons, each characterized by nine basic soil parameters. This study employed the digital version of the soil's physical characteristics to identify soil texture (Pásztor et al., 2018). Soil texture influences several soil properties, including bulk density, water-holding capacity, permeability, and porosity. Soils with sandy textures possess larger pore spaces, enabling rapid rainfall drainage through the soil. Sandy soils have high permeability, resulting in increased infiltration rates and favourable drainage characteristics. On the other hand, clay-textured soils have smaller pore spaces, leading to slower water drainage. Soils predominantly composed of sand particles exhibit higher permeability and lower water-holding capacity than soils with a higher content of loam and clay (Mobilian and Craft, 2022). Forest, lawn, and pasture categories are located mainly (81.6 % and 67.7 %) on sandy soil with highly permeable conditions, α_2; for sterility conditions and factors, α_3, we define the forest category as closed forest. Therefore, based on α_1, α_2, and α_3, the runoff coefficient for forest, lawns and pasture are 11 % and 28 %, respectively. The bare ground category is primarily found in loamy soil (72.25 %) with medium permeability conditions, α_2 and sterility conditions, α_3, being at the boundary of broken cultivable and pasture types, according to Kenessey (1930). Consequently, the considered runoff coefficient for this category is 31 %. Most of the crop-covered area is found on loamy soil (48.4 %), distinguished by permeable soil condition, α_2. According to Kenessey's α_3 factor of broken cultivated soil and light woody shrubs for sterility conditions, the runoff coefficient is 22 %. As Kenessey's study did not specifically address the sealed and semi-sealed classes, the runoff coefficient for these two categories was determined by referencing several additional studies, as presented in Table 6.

Infiltration. In this study, the infiltration presents the weakest link from

Table 4
Crop coefficients (K_c) for the main types of vegetation in Debrecen LC categories (Tallis et al., 2013).

LC categories based on references	K_c based on references	LC categories of Debrecen	K_c for Debrecen
Urban and Built-up	0.001	Sealed surface	0.001
Orchards/Vineyards	0.7	Area with crop cover	0.783
Mixed vegetation cover	1		
Cropland (Row Crops)	0.65		
Wooded Grassland	1	Lawns and pasture	0.833
Grazing Pasture	0.65		
Pasture	0.85		
Urban and Built-up	0.001	Semi-sealed surface	0.26
Bare Ground	0.001		
Wooded Grassland	1		
Open Shrubland	0.398		
Evergreen Needle leaf Forest	1	Forest	1
Evergreen Broad leaf Forest	1		
Bare Ground	0.001	Bare ground	0.001
Open Water and <2 m depth	1.2	SWB	1.2
Open Water and >5 m depth	1		
Stagnant Water	1.4		

Table 5
Summary of Kenessey factors and sub-factors (Kenessey 1928, 1930).

Kenessey 1928, 1930			Mean values [%]
Slope conditions and factors	Very steep slope (> 35 %)	α_1	26
	Steep slope (35 % – 11 %)		16
	Moderate slope (11 % – 3.5 %)		8
	Gentle slope (< 3.5 %)		3
Permeability conditions and factors	Impermeable	α_2	26
	Slightly permeable		16
	Permeable		8
	Very permeable		4
Sterility conditions and factors	Bare rock area	α_3	26
	Pasture		21
	Broken cultivated land and light woody shrubs		11
	Closed forest, loose rubble soil, rocky or sandy deserts		4

Table 6
Runoff coefficients for sealed and semi-sealed LC classes from various studies.

LC Categories	Runoff Coefficient (R%)	Bibliographical references
Forest	11	Kenessey (1928, 1930)
Lawns and Pasture	28	
Area with Crop Cover	22	
Bare Ground	31	
Sealed Surface	82	Lindeburg (1999), Brown et al. (1996); The Comet Program 2010; Musy and Higy (2004); Office cantonal de L'eau (OCEau) (2005); Seto et al. (2011); Town of Buckeye Public Works Department (2007); Malcom (1997); Pontius (2000)
Semi-sealed Surface	66	

the modelling perspective since the infiltration calculation is very complex and requires good understanding of the soil texture. However, since the soil in the urban environment is highly disturbed by human activities, to overcome this problem, the balance equation was used with an unknown parameter: infiltration by the LC category. The infiltration volume for each LC class can be calculated using a balance equation, incorporating a new variable, namely infiltration by LC class. The infiltration ratio can be obtained through the application of Eq. (4) (Batelaan and Smedt, 2001).

$$I = 100 - (ET_{cn} + R) \tag{4}$$

Where,
I is infiltration rate [%],
ET_{cn} is evapotranspiration rate [%], and
I is runoff rate [%].

We considered the runoff $C_R(n)$, infiltration $C_I(n)$ and evapotranspiration coefficient $C_{ET}(n)$ of LC class n (Eq. (5)):

$$\begin{cases} 0 \le C_R(n), C_I(n), C_{ET}(n) \\ C_R(n) + C_I(n) + C_{ET}(n) \end{cases}, \forall n \tag{5}$$

Where,
$C_R(n)$ is LC specific runoff coefficient,
$C_I(n)$ is LC specific infiltration coefficient, and
$C_{ET}(n)$ is LC specific evapotranspiration coefficient.

Where P present the volume of water falling as precipitation in a certain area. In order to produce simple qualitative indicators, we assumed that after an arbitrarily long period of time, this volume of water is divided into three components, which are runoff water, infiltrated water, and evapotranspiration water (Eqs. (6)-8).

$$R(t) = f_R(t)P \tag{6}$$

$$I(t) = f_I(t)P \tag{7}$$

$$ET(t) = f_{ET}(t)P \tag{8}$$

Where,
R is the volume of runoff water of the area [mm],
I is the volume of infiltrated of the area [mm],
ET is the volume of evapotranspirated water of the area [mm],
t is the runoff phase, and
P is the volume of water falling as precipitation on area [mm].

Eq. (6) indicates the portion of the volume of water that after arriving in the form of precipitation on the area passes through a runoff phase. There is no indication of what will happen to the runoff water after that, it may continue to runoff, infiltrate into the ground, absorbed by vegetation, or evaporate. Therefore, we consider the fractions of runoff, infiltration, and evapotranspiration (f_R, f_I andf_{ET}) are simple indicators of trends in the relative importance of the three main hydrological processes runoff, infiltration, and evapotranspiration according to LC (Eq. (9)).

$$\begin{cases} f_R(t) = \sum_{n=1}^{N} C_R(n)a_n(t) \\ f_{ET}(t) = \sum_{n=1}^{N} C_{ET}(n)a_n(t), \\ f_I(t) = \sum_{n=1}^{N} C_I(n)a_n(t) \end{cases} \tag{9}$$

Where,
$C_R(n)$ is LC specific runoff coefficient,
a_n is LC surface,
$C_{ET}(n)$ is LC specific evapotranspiration coefficient, and
$C_I(n)$ is LC specific infiltration coefficient.

Results

Classified lc map

Training data quality assessment of the mapping

Simple measures of separability such as transformed TD are used to assess the statistical separability of a training dataset. This statistical parameter measures the separability between classes in N-dimensional space, where N represents the number of spectral bands.

The separability analysis between all pairs yielded values above 1.9 for J-M and a perfect score of two for the TD distance measures. These results, as displayed in Table 7, indicate excellent separability of the spectral signatures. The high separability values (1.998–2) underscore the effectiveness of the training dataset in capturing the distinct spectral characteristics of various LC classes.

Fig. 5 provides a visual representation of Landsat 8 spectral signatures extracted from the training dataset. This graphical representation aids in understanding the spectral characteristics of each LC category. Within the visible range of the electromagnetic spectrum (EM) each material was only slightly separated as a function of different reflection intensities with semi-sealed surface and area with crop cover the highest reflectance. Forest and SWB was identical even in red wavelength thus could not be separated in this portion of the EM spectrum. All LC categories showed separation in the near-infrared except for forest, bare ground, as well as lawns and pasture. The SWB was characterized by much lower reflectance in band 5 and in SWIR bands than the other LC categories. All LC categories showed reflectance differences except for bare ground and semi-sealed surface in SWIR1 band, as well as bare

Table 7
Spectral signature separability measures for all pairs using J-M.

Class pairs		J-M
Area with crop cover	Sealed surface	2
	Lawns and pasture	2
	Forest	2
	Semi-sealed surface	2
	Bare ground	2
	Surface water bodies	2
Bare ground	Semi-sealed surface	1.998
	Sealed surface	2
	Lawns and pasture	2
	Forest	2
	Surface water bodies	2
Forest	Semi-sealed surface	1.999
	Sealed surface	2
	Surface water bodies	2
	Lawns and pasture	2
Lawns and pasture	Semi-sealed surface	1.999
	Surface water bodies	2
	Sealed surface	2
Sealed surface	Semi-sealed surface	1.999
	Surface water bodies	2
Semi-sealed surface	Surface water bodies	2

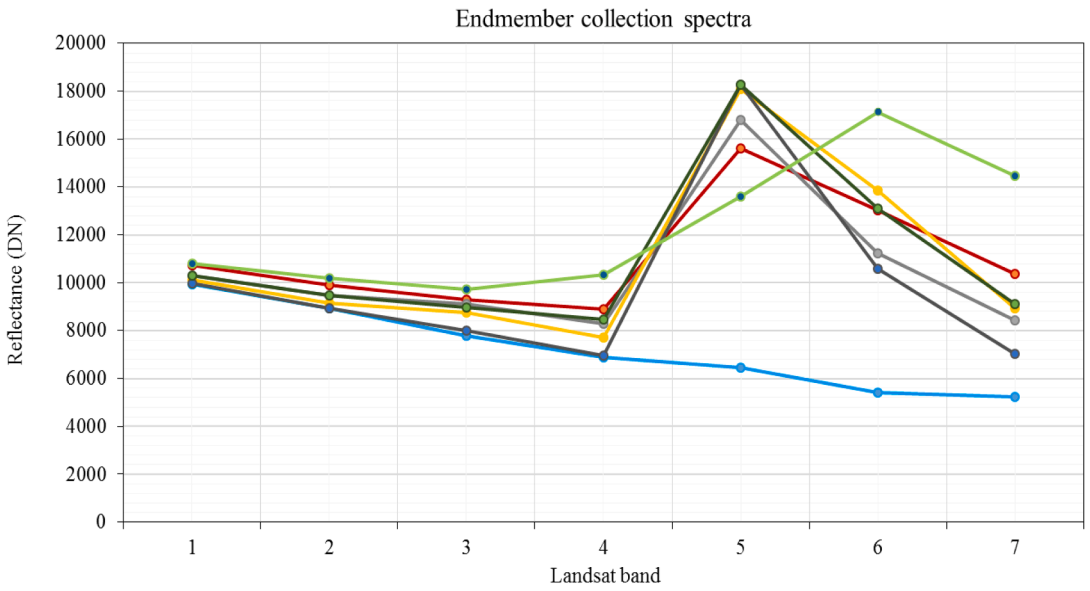

SD	(coastal aerosol) 0,43µm	(blue) 0,45µm	(green) 0,53µm	(red) 0,64µm	(NIR) 1,85µm	(SWIR1) 1,57µm	(SWIR2) 2,1µm
SWB	15	12	19	23	20	18	19
semi seald surface	201	245	313	570	1 270	742	813
sealed surface	81	101	198	205	1 311	579	598
lawns and pasture	31	33	42	97	547	158	112
forest	16	17	38	36	314	210	73
bare ground	61	118	123	536	1 119	800	690
area with crop cover	33	54	97	154	252	190	111

Fig. 5. Plot of spectral reflectance for LANDSAT 8 bands 1, 2, 3, 4, 5, 6 and 7 with standard deviation (SD) values.

ground and lawns and pasture in SWIR2 band. In SWIR bands area with crop cover showed the highest EM intensity. Notably, semi-sealed surfaces exhibit the highest SD values, ranging from 200 to 1269. Conversely, water body surfaces demonstrate the lowest SD, 12 to 23. This is due to the extreme homogeneity of water surfaces, resulting in minimal mixing of pixels. In contrast, semi-sealed surfaces display greater variability, with pixels appearing more dispersed or mixed (Fig. 5).

Validation and LC mapping in Debrecen

To assess the quality of the resulting LC map, the classification accuracy was initially investigated. The OA of the classification results is 81.2 % with a kappa index greater than 0.78, which shows that 81.2 % of the 770 observation areas (110 per cover category) are correctly classified, while 18.8 % are incorrectly classified. In addition, the model performs well since it may be used when a classification model's kappa index is between 0.50 and 0.75 (Sajjad et al., 2022). These statistics assume that our classifications are accurate and representative of reality. The model performance concerning each LC class was also assessed using the F1-score (per class) metric (Talha et al., 2023).

The most balanced and highest F1 score was achieved by forest, semi-sealed area, and surface water body classes with values of 0.971, 0.940, and 0.908, respectively. The LC classes characterized by crop cover, lawns and pasture exhibited the lowest and most imbalanced F1-scores, indicating potential signal mixture issues during the classification process. Specifically, the F1-scores for crop cover, lawns and pasture were recorded as 0.647 and 0.668, respectively (Table 8).

In addition to errors from the classification itself, other sources of errors, such as poor quality of training or test samples, interpretation errors, and position errors resulting from the registration, all affect classification accuracy. In the process of accuracy assessment, it is commonly assumed that the difference between an image classification result and the reference data is due to the classification error. For example, the geographical and radiometric resolution limitations of RS data, as well as the atmospheric conditions at the time of image collecting, may generate uncertainty in RS data. Geometric rectification or image registration between multisource data may also result in position uncertainty, while approaches used to calibrate atmospheric or topography factors may result in radiometric errors (Lu et al., 2008). As an example, the actual LC map and related hydrological parameters for the year 2019 are introduced. The LC distribution displayed in Fig. 6 demonstrates significant variation across different areas.

Table 8
Accuracy assessment: kappa error matrix resulting from classifying test pixels.

LC category	Users' accuracy [%]	Producers' accuracy [%]	F1 score
Surface water body	83.3	100	0.908
Lawns and pasture	64	70	0.668
Forest	94.4	100	0.971
Semi-sealed surface	88.8	100	0.940
Area with crop cover	63	66.6	0.647
Bare Ground	83.3	63.6	0.721
Sealed surface	88.8	72.7	0.799

Forests dominate the northern and eastern regions, while crop-covered areas constitute the largest proportion of LC within the watershed. The urban area is primarily concentrated in the central part of the basin. According to Table 9 presenting the distribution of LC classes in the study area, the dominant LC class is crop-covered areas, occupying 32.78 % of the entire region, equivalent to 15,120.22 hectares. It is important to note that both Crop Cover and Bare Ground areas are used for crop production. Forests, covering 30.26 % of the total area (13,958.05 hectares), also have a significant presence in the LC distribution. The sealed surface area, mainly located in the central part of the basin, represents 1.5 % of the region's area, corresponding to 692.46 hectares. Lawns and pasture cover a large area of 9415.21 hectares,

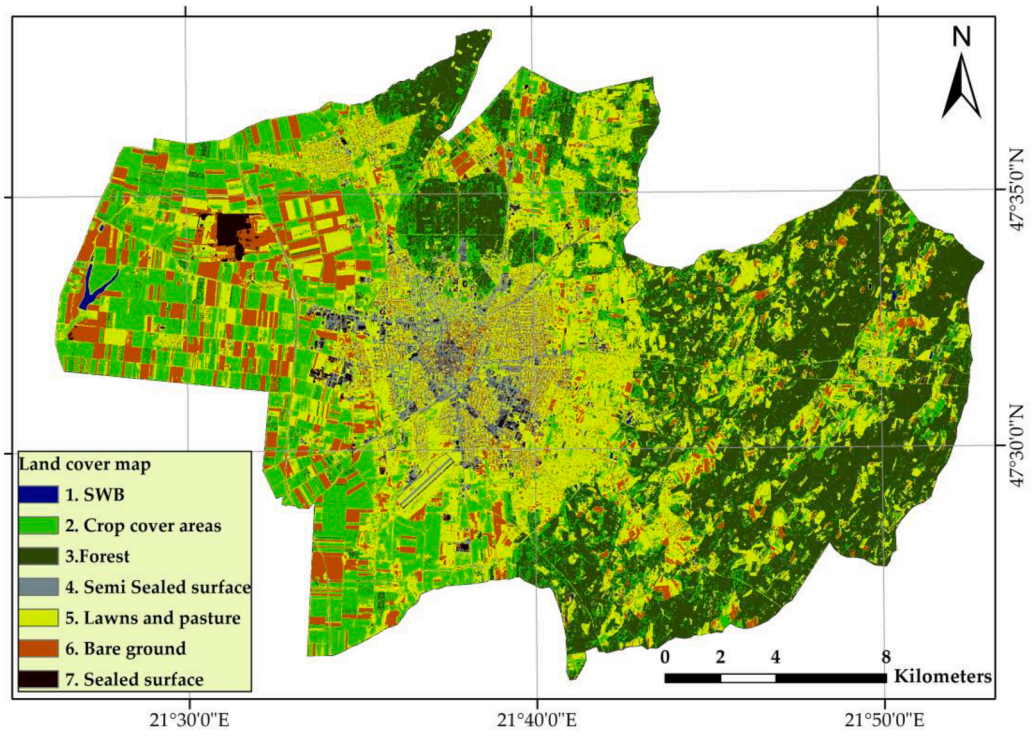

Fig. 6. LC map for Debrecen based on Landsat 8 data (19/06/2019).

Table 9
Area and percentage of different LC categories in Debrecen basin.

LC category	Area [ha]	Proportion [%]
Surface water body	82.65	0.17
Lawns and pasture	9415.21	20.41
Forest	13,958.05	30.26
Semi-sealed surface	2149.53	4.66
Area with crop cover	15,120.22	32.78
Bare Ground	4698.1	10.18
Sealed surface	692.46	1.5
Total	**46,116.25**	**100**

accounting for 20.41 % of the total, while bare ground covers 10.18 % or 4.698 hectares. The research of Iváncsics and Kovács (2021) indicates that the sealed surface area in Debrecen expanded by 285.9 hectares between 2000 and 2006. This growth can be attributed to Debrecen's increasing population, boosting economy, and infrastructure development. Urban expansion has placed significant pressure on agricultural land within cities (Tarawally et al., 2019). In our study area, the main crops cultivated are wheat and corn, and after each harvest, the fields are typically rotated to bare ground. Consequently, the bare ground and crop cover categories are dynamic and can vary throughout the year and between years due to crop rotation. In contrast, forests represent a stable LC type that remains consistent throughout the year, regardless of seasonal changes.

LC and hydrological parameters relationship

To illustrate the impact of LC on hydrological parameters (Fig. 3), this section examines the specific relationships observed in the Debrecen basin. It is important to highlight that the research area exhibits a predominantly flat topography, and the LC map was derived during the high biomass and vitality period of summer (July). However, it should be noted that plant cover can undergo changes in different seasons throughout the year (Hüse et al., 2016). The significance of this study lies in the fact that, despite potential variations in crop patterns, the computation and validation process can be applied to different locations and time periods. The evapotranspiration, runoff, and infiltration coefficients are expressed as mean annual precipitation volume percentages. The results of the hydrological parameters for each LC category in the Debrecen basin are presented in Table 10.

The SWB class exhibits the highest evapotranspiration ratio, ranging from 83.4 % to 88.59 %. This is primarily due to direct exposure to solar radiation, which leads to significant water evaporation. In the case of a surface water body, the infiltration ratio was not considered, as the water infiltrating into watercourse beds primarily originates from catchment runoff rather than precipitation. Consequently, the runoff of the surface water body was calculated solely based on the evapotranspiration percentage, which ranges from 11.41 % to 16.6 %, with an average of 14 %.

Our model estimates the evapotranspiration values for the forest category to be between 69.54 % and 73.82 %. The sealed surface, semi-sealed, and bare ground categories have relatively high runoff ratios. This is attributed to the absence of vegetation, which reduces the capacity for water retention and increases water runoff. On the other hand, forests, areas with crop cover, and lawns and pasture demonstrate limited runoff, highlighting the crucial role of vegetation in mitigating water runoff. Specifically, the sealed surface areas exhibit a high runoff coefficient of 82 % but have a very low evapotranspiration coefficient of 7.127 %. The runoff coefficient is 66 % for the semi-sealed areas, while

Table 10
Hydrological parameters by LC category.

LC category	Evapotranspiration ratio		Infiltration Ratio
	Min-Max [%]	Average [%]	Average [%]
Surface water body	83.40 - 88.59	85.99	–
Lawns and pasture	57.90 - 61.40	59.65	12.35
Forest	69.54 - 73.82	71.68	17.32
Semi-sealed surface	18.00 - 19.19	18.59	15.40
Area with crop cover	54.45 - 57.80	56.12	21.87
Bare ground	06.95 - 07.38	7.165	61.83
Sealed surface	06.95 - 07.30	7.127	10.87

the evapotranspiration coefficient is 18.59 %. The highest mean annual evapotranspiration percentages were recorded in the surface water body and forest LC classes, with values of 85.99 % and 71.68 %, respectively. Conversely, the sealed surface area and bare ground class exhibited the lowest evapotranspiration percentages, with values of 7.127 % and 7.16 %, respectively.

The mean annual runoff percentage for the semi-sealed area is 66 %, while the sealed surface area shows a remarkably high runoff percentage of 82 %. The crop-covered area has a runoff percentage of 22 % of the total annual precipitation. The forest and bare ground classes exhibit mean annual runoff percentages of 11 % and 31 %, respectively. This can be attributed to the impact of urban LC, which increases storm water runoff by reducing vegetative cover and increasing impervious surfaces. The high ratio of evapotranspiration and surface runoff above groundwater recharge in the basin demonstrates the need for significant effort to change the environmental conditions of the basin to promote groundwater recharge through a variety of mechanisms, whereby the high amount of surface runoff may be used to design artificial recharge structures. Regarding infiltration values, the forest, pasture, and crop-covered areas recorded infiltration percentages of 17.32 %, 12.35 %, and 21.875 %, respectively. The infiltration value of sealed surface areas is 10.87 % emphasizing the importance of plants and vegetation cover in facilitating infiltration.

Discussion

LC classification method

Landsat 8′s ability to distinguish between different LC classes is attributed to its spectral bands, this spectral information allows Landsat 8 to effectively differentiate between vegetation, water, and other LC types (Roy et al., 2016a). For example, vegetation typically has high reflectance in the near-infrared (NIR) band and low reflectance in the red band, while water has high reflectance in the blue band and low reflectance in the red and NIR bands (Mondejar and Tongco, 2019). In our study, we demonstrated that Landsat 8 effectively distinguished between different LC classes, achieving high classification accuracy for all investigated LC classes. We achieved F1 scores ranging from 0.64 for crop-covered areas to 0.97 for forest, aligning well with the accuracies reported in other studies utilizing Landsat 8 for LC classification (Jia et al., 2014; Sajjad et al., 2022).

Similar to our study, the scientific literature highlights the frequent occurrence of confusion among classes that exhibit apparent similarities. Sajjad et al. (2022) reported F1 scores of 0.926 for areas with crop cover, 0.848 for sealed surface sites, 0.927 for bare ground, and 0.937 for surface water bodies (in district Okara) using the same Landsat 8 and MLSC approach. The authors emphasized that grassland and cultivated land exhibited the lowest producer and OA values during the classification accuracy testing. As in the case of this study, this was attributed to misclassified patches, where specific areas of cultivated land were mistakenly categorized as grassland. To tackle this issue, other studies noted the need for revising the OLI photos from 16/04/2015, 22/08/2015, and 25/10/2015 to capture the complete phenology of vegetation (Guiying et al., 2012). In a moist tropical region of Brazil, Guiying et al. (2012) found better vegetation classification performance by combining different vegetation indices. For better classification of vegetation the necessity of integrating the combinations of two or more vegetation indices (NDVI, Enhanced Vegetation Index (EVI), Soil-Adjusted Vegetation Index (SAVI)) were emphasized to improve vegetation classification performance by comparing the outcomes of the above three studies (Hungary, Europe; Pakistan, Asia; and Brazil, South America) (Matsushita et al., 2007; Lee et al., 2021). Lu et al. (2008) proposed to identify the best combination based on TD values and correlation coefficients.

In this study, we present an improved approach for updating LC maps using MLSC classifier. We integrate the LC map with calculated hydrological parameters to enhance the accuracy and robustness of the methodology. On the other hand, the choice of classification method (e.g., MLSC, Random Forest (RF) and Support Vector Machine (SVM)) can also affect performance and the accuracy of the classification. Several studies reported minor to moderate fluctuation (ranging from 71 % to 93 %) in the OA of the LC classification using different classifiers (e.g. MLSC, RF and SVM) (Basheer et al., 2022; Talukdar et al., 2020; Adugna et al., 2022). Ghosh et al. (2014) reported a lower OA of 69 % and a Kappa index of 0.65 for a RF machine learning classification of nine LC categories in India. This suggests the MLSC method used in the present study achieved superior performance. However, their study highlights the challenges associated with LC classification. specifically, the misclassification of forests and plantations as double crops due to similar spectral signatures and phenology compromised their classification process, resulting in a producer accuracy of only 33 % for plantations and 60 % for forests.

Another classification approach is the SVM, which presents a set of supervised learning methods for classification, regression, and outlier detection (Shi and Yang, 2015). While our approach has shown promising results, several studies have demonstrated the effectiveness of SVMs in LC classification (Deilmai et al., 2014; Abbas et al., 2020). According to their findings, the OA and Kappa index for SVM classification are 86 % and 0.92, as well as 90 % and 0.95, respectively. Given the promising results of SVMs in this domain, we plan to investigate the integration of hydrological parameters with LC mapping using SVM classification in the future. The integration of hydrological parameters with SVM classification is expected to provide a more comprehensive and precise representation of LC types and their relationships to hydrological conditions.

Hydrological properties

Previous studies provide insights into pan coefficients for determining evaporation rates for different regions and for different LC types. For instance, Abtew (2001) utilized seven pan stations to establish pan coefficients for Lake Okeechobee in South Florida, reporting an average coefficient of 0.76, ranging from 0.64 to 0.95 annually. Boyd (1985) conducted a well-controlled experiment at Auburn, Alabama, and reported pond-to-pan evaporation coefficients ranging from 0.72 to 0.90, with an average of 0.81. Morton (1986) applied the Complementary Relationship Lake Evaporation (CRLE) model to study the evaporation of 16 lakes in North America and one lake in East Africa. By extracting pan coefficients from reported pan evaporation and CRLE lake evaporation estimates, a range of coefficients for the 17 lakes was obtained, with a mean of 0.69 and coefficients ranging from 0.59 to 0.84.

Zhou et al. (2002) reported that in southern China well-forested eucalyptus plantations could exhibit evapotranspiration rates as high as 90 % of the annual precipitation which are higher than those of deciduous forests in Debrecen. This is due to the difference in climate and the type of vegetation, since in Debrecen the main dominant species are Quercus species, Populus species, Pinus species and Robinia pseudoacacia.

The decrease in the evapotranspiration coefficient in urban areas can be attributed to reduced vegetation and increased storm water runoff due to the expansion of impervious surfaces (Hung et al., 2018). Numerous studies have supported the conclusion that evapotranspiration rates in urban areas are generally low due to a decrease in green space (Hao et al., 2018; Qiu et al., 2017). Converting croplands to urban use reduces surface roughness, vegetation leaf area and rooting depth, thus reduces ecosystem ET rates (Sampaio et al., 2007).

A form of non-stationarity known as percent impervious area, backwater behind bridges, storm sewer systems, and other changes to runoff generation and storm-water conveyance can lead to increased runoff and flood risks as a result of urbanization. The statistical characteristics of hydrologic events, such as the mean or variance of rainfall or streamflow, can alter under non-stationary conditions. It can be

caused by internal climate fluctuation, human activity, and natural or anthropogenic climate change (Milly et al., 2008). Independent of anticipated future changes in precipitation intensity that may be caused by climate change, the considerable increases in runoff and discharge shown by this study suggest that urbanization is a critical driver of increased flood risks in developed areas. In our study, we found that the forest class has the lowest runoff rate (11 %), demonstrating the advantages of vegetation cover in lowering runoff and flood risk. There is a direct relationship between vegetation cover and infiltration rate, with the higher infiltration rate being shown by the bare ground class at 65.83 %. Studies investigated the effects of forest cover change on streamflow components by varying degrees of reforestation or deforestation, concluding that forest cover reduction and soil sealing can lead to an increase in surface runoff and flash floods in cities and an increase in groundwater level. As the forest is harvested, the groundwater table increases, although the magnitude and duration of this increase will vary depending on the geology and topography of the area (Smerdon et al., 2009). Eucalyptus plantations reduced groundwater recharge, according to research on reforestation in southern India (Calder et al., 1992).

Other researchers have utilized hydrological models to investigate how changes in LC or forest cover affect different runoff components, however, they came to various conclusions (Zhou et al., 2002). For example, in south-western China, a research employing the SWAT indicated that increased vegetation cover considerably reduced total and surface runoff while increasing base flow (Ma et al., 2009). In contrast, in the Be River Basin, Vietnam, a research demonstrated that a decrease of forest cover increased total and surface runoff and reduced base flow (Nguyen and Tadashi, 2012). These contrasting results show that runoff components are significantly affected by changes in forest cover or LC, and they suggest the need for additional studies to better understand the hydrological response properties of streamflow components. Therefore, our findings have significant implications for the designing of the implementations of green infrastructural innovations in urban sites, assisting in the management of water resources and the preservation of ecosystems in watersheds.

Conclusion

Integrated water resources management is a complex field that requires extensive data and a comprehensive understanding of natural systems and their interactions with socio-hydrological components. Understanding the relationships between LC and vital hydrological processes within the water cycle is crucial in this context. The implication of complex data collection and processing, the developed LC classification method for the study area and hydrological coefficient calculations for each LC categories defining urban water balance were proved to be a good tool for the estimation of the hydrological cycle parameters on pixel scale, as well as, on a larger scale in the case of each LC category. In details, the study demonstrated the feasibility of using Landsat 8-based LC classification to identify hydrological parameters at the pixel level. Notably, the spectral signatures exhibited excellent separability with values ranging from 1.998 to 2, further highlighting the effectiveness of the training dataset in capturing the distinct spectral characteristics of various LC classes. MLSC algorithm was used successfully to classify LC, achieving an impressive OA of 81.2 %. This high accuracy suggests that the data used possessed well-defined spectral signatures, making it well-suited for the MLSC approach. The present research also highlights the potential of using this tool for LC planning and integrated water resources management at the urban watershed scale supporting decision-makers and water resource managers.

However, it is essential to acknowledge certain limitations of this method, Firstly, the 30 m resolution of Landsat data used may not capture fine scale patterns, and the classification process may lead to pixel intermingling. Future studies using higher resolution imagery (i.e. Sentinel 2) or LiDAR data could capture these nuances and potentially refine the analysis. Secondly, while GE verification served its purpose, ground-truthing through field surveys remains the gold standard. Prioritizing field data collection in future research will ensure the accuracy and robustness of findings. Additionally, the calculated hydrological parameters require validation with in-situ measurements. Besides there are other methods, (e.g. ML algorithms) for LC classification that can be he integrated with hydrological parameters which may provide a more comprehensive and precise LC categorization, resulting in better monitoring of hydrological conditions in urban areas. Integrating these measurements, in future studies will refine the calculations and enhance model accuracy. Furthermore, expanding the methodology to include additional hydrological parameters like water storage and utilizing more precise meteorological data can offer a more comprehensive picture of system's dynamics. Finally, exploring potential LC changes and incorporating future meteorological projections into the model can provide valuable insights into potential future hydrological responses, informing adaptation strategies. By acknowledging these limitations and outlining these future research directions, this study not only presents valuable findings but also lays the groundwork for further advancements.

In summary, a rapid, quick and quasi-real-time LC mapping method was introduced to provide a good example for a tool to investigate urban and industrial sprawl pattern in middle-sized cities in the region. The LC mapping method combined with hydrological calculations contributes to improved monitoring and design of up-to-date hydrologic properties for rapidly developing urban regions.

CRediT authorship contribution statement

Douraied Guizani: Writing – original draft, Visualization, Validation, Software, Methodology. **Erika Buday-Bódi:** Writing – original draft, Validation, Software, Methodology, Formal analysis, Conceptualization, Visualization. **János Tamás:** Formal analysis, Data curation, Funding acquisition, Supervision. **Attila Nagy:** Writing – review & editing, Writing – original draft, Software, Resources, Project administration, Conceptualization, Methodology.

Declaration of competing interest

The authors declare that they have no known competing financial interests or personal relationships that could have appeared to influence the work reported in this paper.

Data availability

Data will be made available on request.

Acknowledgment

The research presented in the article was carried out within the framework of the Széchenyi Plan Plus program with the support of the RRF 2.3.1 21 2022 00008 project.

References

Abbas, Z., Jaber, H.S., 2020. Accuracy assessment of supervised classification methods for extraction land use maps using remote sensing and GIS techniques. IOP Conf. Ser.: Mater. Sci. Eng. 745, 012166 https://doi.org/10.1088/1757-899X/745/1/012166.

Abtew, W., 2001. Evaporation estimation for lake Okeechobee in South Florida. J. Irrig. Drain. Eng. 127 (3), 140–147. https://doi.org/10.1061/(ASCE)0733-9437(2001)127:3(140).

Acharki, S., 2022. Planet Scope contributions compared to Sentinel-2, and Landsat-8 for LULC mapping. RSASE 27. https://doi.org/10.1016/j.rsase.2022.100774.

Adugna, T., Xu, W., Fan, J., 2022. Comparison of random forest and support vector machine classifiers for regional land cover mapping using coarse resolution FY-3C images. Remote Sens. 14 (3), 574. https://doi.org/10.3390/rs14030574.

Ahmad, A., Quegan, S., 2012. Analysis of maximum likelihood classification on multispectral. Appl. Math. Sci. 6 (129), 6425–6436. Available online. https://www.researchgate.net/publication/279541271_Analysis_of_maximum_likelihood_classification_on_multispectral_data.

Al Kafy, A., Bakshi, A., Saha, M., Al Faisal, A., Almulhim, A.I., Rahman, Z.A., Mohammad, P., 2023. Assessment and prediction of index based agricultural drought vulnerability using machine learning algorithms. Sci. Total Environ. 867, 161394 https://doi.org/10.1016/j.scitotenv.2023.161394.

Al Kafy, A., Saha, M., Al Faisal, A., Rahman, Z.A., Rahman, M.T., Liu, D., Fattah, M.A., Al Rakib, A., AlDousari, A.E., Rahaman, S.N., Zakaria, M.H., Ahasan, M.K.A., 2022. Predicting the impacts of land use/land cover changes on seasonal urban thermal characteristics using machine learning algorithms. Build Environ 217, 109066. https://doi.org/10.1016/j.buildenv.2022.109066.

Ali, M.Z., Qazi, W., Aslam, N., 2018. A comparative study of ALOS-2 PALSAR and landsat-8 imagery for land cover classification using maximum likelihood classifier. Egypt. J. Remote. Sens. Space Sci. 21, S29–S35. https://doi.org/10.1016/j.ejrs.2018.03.003.

ASTER Science Team, 2013. ASTER Data Available at no Charge. Land Processes Distributed Active Archive Center. Retrieved from. https://lpdaac.usgs.gov/tools/.

Asuquo, E.M., Ebere, N.R., Chinenye, O.U., 2023. Modeling and mapping the spatial temporal changes in land use and land cover in Lagos: a dynamics for building a sustainable urban city. Adv. Space Res. 72 (3), 694–710. https://doi.org/10.1016/j.asr.2022.07.042.

Bakacsi, Z., Laborczi, A., Szabó, J., Takács, K., Pásztor, L., 2014. Proposed correlation between the legend of the 1:100.000 scale geological map and the FAO code system for soil parent material. Agrokémia és Talajtan 63 (2), 189–202. https://doi.org/10.1556/agrokem.63.2014.2.3.

Barranco, R., Silva, F.B.E., Herrera, M.M., Lavalle, C., 2014. Integrating the MOLAND and the urban atlas geo-databases to analyze urban growth in European cities. J Map Geogr Libr 10 (3), 305–328. https://doi.org/10.1080/15420353.2014.952485, 673.

Basheer, S., Wang, X., Farooque, A.A., Nawaz, R.A., Liu, K., Adekanmbi, T., Liu, S., 2022. Comparison of land use land cover classifiers using different satellite imagery and machine learning techniques. Remote Sens. 14, 4978. https://doi.org/10.3390/rs14194978.

Batelaan, O., Smedt, F., 2001. WetSpass: a flexible, GIS based, distributed recharge methodology for regional groundwater modelling. IAHS-AISH 269, 11–18b. https://www.researchgate.net/publication/251732752_WetSpass_A_flexible_GIS_based_distributed_recharge_methodology_for_regional_groundwater_modelling.

Bayraktar, S., Cegielska, K., Sökmen, E.D., Noszczyk, T., Yener, Ş.D., Kukulska-Kozieł, A., 2024. Directions of land degradation in the greater Istanbul metropolitan area: a view from four decades. Land Degrad. Develop. 35 (5), 1656–1672. https://doi.org/10.1002/ldr.5012.

Blaschke, T., 2010. Object based image analysis for remote sensing. ISPRS J. Photogramm. Remote Sens. 65 (1), 2–16. https://doi.org/10.1016/j.isprsjprs.2009.06.004.

Bolstad, P.V., Lillesand, T.M., 1991. Rapid maximum likelihood classification. Photogrammet. Eng. Remote Sens. 57, 67–74.

Borsy, Z., 1989. Az Alföld hordalékkúpjainak negyedidőszaki fejlődéstörténete. Földrajzi Értesítő 38, 211–224.

Boulila, W., Sellami, M., Driss, M., Al-Sarem, M., Safaei, M., Ghaleb, F.A., 2021. RS-DCNN: A novel Distributed Convolutional-Neural-Networks Based-Approach For Big Remote-Sensing Image Classification, 182. Computers and Electronics in Agriculture. https://doi.org/10.1016/j.compag.2021.106014.

Boyd, C.E., 1985. Pond evaporation. Trans. Am. Fish. Soc. 114 (2), 299–303. https://doi.org/10.1577/1548-8659(1985)114%3C299:PE%3E2.0.CO;2.

Brodmann, T., 2016. Drinking Water Risk Treatment Plan (In Hungarian –IVÓVÍZBIZTONSÁGI TERVEK KÉSZÍTÉSE) Országos Közegészségügyi Központ –Országos Környezetegészségügyi Igazgatóság. Lecture notes. 27/06/2016.

Brown, S.A., Stein, S.M., Warner, J.C., 1996. Urban drainage design manual. Hydraulic Engineering Circular 22, FHWA-SA-96-078, 3rd ed. Federal Highway Administration, and U.S. Department of Transportation: Washington DC. Available online https://rosap.ntl.bts.gov/view/dot/54350/dot_54350_DS1.pdf.

Bruse, M., Fleer, H., 1998. Simulating surface–plant–air interactions inside urban environments with a three dimensional numerical model. Environ. Model. Softw. 13 (3–4), 373–384. https://doi.org/10.1016/S1364-8152(98)00042-5.

Bruzzone, L., Prieto, D.F., 2001. Unsupervised retraining of a maximum likelihood classifier for the analysis of multi temporal remote sensing images. IEEE Trans. Geosci. Remote Sens. 39 (2), 456–460. Available online. https://ieeexplore.ieee.org/document/905255.

Buday-Bódi, E., Buday, T., Magyar, T., Molnár, L., Tamás, J., 2019. Possible environmental aspects of thermal water utilisation in northeast Hungary. Nat. Resour. Sustain. Develop. 9 (1), 17–26. https://doi.org/10.31924/nrsd.v9i1.019.

Calder, I.R., Swaminath, M.H., Kariyappa, G.S., Srinivasala, N.V., Srinivasala, K.V., Mumtaz, J., 1992. Deuterium tracing for the estimation of transpiration from trees. J. Hydrol. 130 (1–4), 37–47. https://doi.org/10.1016/0022-1694(92)90102-2.

Chemak, F., Nouir, I., Bellali, H., Chahed, M.K., 2022. Irrigation practices, prevalence of leishmaniasis and sustainable development: evidence from the Sidi Bouzid region in central Tunisia. Sci. Afr. 15 https://doi.org/10.1016/j.sciaf.2022.e01094.

Cieślak, I., Biłozor, A., Szuniewic, K., 2020. The use of the CORINE land cover (CLC) database for analyzing urban sprawl. Remote Sens. 12, 282. https://doi.org/10.3390/rs12020282.

Cohen, J.A., 1960. Coefficient of agreement for nominal scales. Educ. Psychol. Meas. 20 (1), 37–46.

Daba, M.H., You, S., 2022. Quantitatively assessing the future land-use/land-cover changes and their driving factors in the upper stream of the awash river based on the CA–Markov model and their implications for water resources management. Sustainability 14 (3). https://doi.org/10.3390/su14031538, 10.3390/su14031538.

Dams, J., Dujardin, J., Reggers, R., Bashir, I., Canters, F., Batelaan, O., 2013. Mapping impervious surface change from remote sensing for hydrological modelling. J. Hydrol. 485, 84–95. https://doi.org/10.1016/j.jhydrol.2012.09.045.

Deilmai, B.R., Ahmad, B.B., Zabihi, H., 2014. Comparison of two classification methods (MLC and SVM) to extract land use and land cover in Johor Malaysia. IOP Conf. Ser.: Earth Environ. Sci. 20, 012052 https://doi.org/10.1088/1755-1315/20/1/012052.

Diouf, O.C., Weihermüller, L., Ba, K., Faye, S.C., Faye, S., 2016. Estimation of Turc reference evapotranspiration with limited data against the Penman-Monteith Formula in Senegal. JAEID 110 (1). https://doi.org/10.12895/jaeid.20161.417.

Dou, P., Huang, C., Han, W., Hou, J., Zhang, Y., Gu, J., 2024. Remote sensing image classification using an ensemble framework without multiple classifiers. ISPRS J. Photogrammet. Remote Sens. 208, 190–209. https://doi.org/10.1016/j.isprsjprs.2023.12.012.

Duarte, L., Teodoro, A.C., Gonçalves, J.A., Guerner Dias, A.J., Espinha Marques, J., 2015. A dynamic map application for the assessment of groundwater vulnerability to pollution. Environ. Earth Sci. 74 (3), 2315–2327. https://doi.org/10.1007/s12665-015-4222-0.

European Environment Agency, 2023a. Corine Land Cover. https://land.copernicus.eu/en/products/corine-land-cover [Online]. Available from. https://land.copernicus.eu/en/products/corine-land-cover.

FAO, 2000. On Definitions of Forest and Forest Change. Forest Resources Assessment Programme 2000, Rome (Italy), Forestry Dept. Working Paper 33, 14 p. Available online: https://www.fao.org/forestry/4036-0a4d4289d7a629dd821f1ce032a83596b.pdf.

Feizizadeh, B., Darabi, S., Blaschke, T., Lakes, T., 2022. QADI as a new method and alternative to kappa for accuracy assessment of remote sensing-based image classification. Sensors 22 (12), 4506. https://doi.org/10.3390/s22124506.

Foody, G.M., 2006. The evaluation and comparison of thematic maps derived from remote sensing. In: 7th International Symposium on Spatial Accuracy Assessment in Natural Resources and Environmental Sciences, pp. 18–31.

Foody, G.M., 2020. Explaining the unsuitability of the kappa coefficient in the assessment and comparison of the accuracy of thematic maps obtained by image classification. Remote Sens. Environ. 239, 111630 https://doi.org/10.1016/j.rse.2019.111630.

Frank, M., Benon, B., 2016. The centrality of water resources to the realization of Sustainable Development Goals (SDG). A review of potentials and constraints on the African continent. ISWCR 4 (3), 215–223. https://doi.org/10.1016/j.iswcr.2016.05.004.

Ghosh, A., Sharma, R., Joshi, P.K., 2014. Random forest classification of urban landscape using Landsat archive and ancillary data: combining seasonal maps with decision level fusion. Appl. Geogr. 48, 31–41. https://doi.org/10.1016/j.apgeog.2014.01.003.

Guha, B., Momtaz, Z., Al Kafy, A., Rahaman, Z.A., 2022. Estimating solid waste generation and suitability analysis of landfill sites using regression, geospatial, and remote sensing techniques in Rangpur, Bangladesh. Environ. Monit. Assess. 195 (52) https://doi.org/10.1007/s10661-022-10695-4.

Guiying, L., Dengsheng, L., Emillio, M., Scott, H., 2012. Land-cover classification in a moist tropical region of Brazil with Landsat TM imagery. Int. J. Remote Sens. 32 (23), 8207–8230, 10.1080%2F01431161.2010.532831.

Hao, L., Huang, X., Qin, M., Liu, Y., Li, W., Sun, G., 2018. Ecohydrological processes explain urban dry island effects in a wet region, southern China. Water Resour. Res. 54 (9), 6757–6771. https://doi.org/10.1029/2018WR023002.

Hardi, T., Repaská, G., Veselovský, J., Vilinová, K., 2020. Environmental consequences of the urban sprawl in the suburban zone of Nitra: an analysis based on land over data. Geogr. Pannonica. 24 (3), 205–220. https://doi.org/10.5937/gp24-25543.

Hermosilla, T., Wulder, M.A., White, J.C., Coops, N.C., Hobart, G.W., 2018. Disturbance-informed annual land cover classification maps of Canada's forested ecosystems for a 29-year Landsat time series. Can. J. Remote. Sens. 44 (1), 67–87. https://doi.org/10.1080/07038992.2018.1437719.

Hung, C.L.J.L., James, A., Carbone, G.J., 2018. Impacts of urbanization on stormflow magnitudes in small catchments in the Sand hills of South Carolina, USA. Anthropocene. 23, 17–28. https://doi.org/10.1016/j.ancene.2018.08.001.

Hüse, B., Szabó, S., Deák, B., Tóthmérész, B., 2016. Mapping an ecological network of green habitat patches and their role in maintaining urban biodiversity in and around Debrecen city (Eastern Hungary). Land Use Policy 57, 574–581. https://doi.org/10.1016/j.landusepol.2016.06.026.

Iváncsics, V., Kovács, K.F., 2021. Analyses of new artificial surfaces in the catchment area of 12 Hungarian middle-sized towns between 1990 and 2018. Land Use Policy 109, 105644. https://doi.org/10.1016/j.landusepol.2021.105644.

Jamshid, T., Nasser, L., Mina, F., 2013. Satellite Image Classification Methods and Landsat 5TM Bands. Department of Computer Engineering EMU University, North Cyprus Famagusta. https://doi.org/10.48550/arXiv.1308.1801.

Jensen, J.R., 2000. Introductory Digital Image processing: a Remote Sensing perspective, 3rd ed. Prentice- Hall Inc, New Jersey.

Jia, K., Wei, X., Gu, X., Li, B., 2014. Land cover classification using Landsat 8 operational land imager data in Beijing, China. Geocarto Int. 29 (8) https://doi.org/10.1080/10106049.2014.894586.

Kashyap, P.S., Panda, R.K., 2001. Evaluation of evapotranspiration estimation methods and development of crop-coefficients for potato crop in a sub-humid region. Agricult. Water Manag. 50 (1), 9–25. https://doi.org/10.1016/S0378-3774(01)00102-0.

Kenessey, B., 1928. The lake balaton. Hungarian: A Balaton) 43 p.

Kenessey, B., 1930. Runoff coefficients and retentions. A hydrological study. Hungarian: Lefolyási tényezők és Retenciók 12, 55–76.

Kim, S., Kim, J., Kang, H., Jang, W.S., Lim, K.J., 2022. Analysis of water balance changes and parameterization reflecting soil characteristics in a hydrological simulation program-FORTRAN model. Water MDPI 14 (6). https://doi.org/10.3390/w14060990.

Klein, I., Gessne, U., Kuenzer, C., 2012. Regional land cover mapping and change detection in Central Asia using MODIS time-series. Appl. Geogr. 35 (1–2), 219–234. https://doi.org/10.1016/j.apgeog.2012.06.016.

Kovács, F., 2011. Az alföldi területhasználat és változásainak értékelése. In: Rakonczai, J. (Ed.), Környezeti Változások és az Alföld. Nagyalföld Alapítvány Kötetei 7. Nagyalföld Alapítvány, Békéscsaba, pp. 159–166.

Kovács, Z., Farkas, J., Egedy, T., Kondor, A., Szabó, B., Lennert, J., Baka, D., Kohán, B., 2019. Urban sprawl and land conversion in post-socialist cities: the case of metropolitan Budapest. Int. J. Urban Policy Plan. 92, 71–81. https://doi.org/10.1016/j.cities.2019.03.018.

Kozma, G., Molnár, E., 2018. The role of industrial parks in the economic development of Debrecen. Tér Gazdaság Ember. 4, 35–49. ISSN 2064-1176.

Kozma, G., Molnár, E., 2021. Debrecen. Nagyvárosok Magyarországon, pp. 125–140 book chapter in Rechnitzer, J., 2021ISBN: 9789635313433; 9789635313426; 9789635313440 pp.

2021 Lee, G., Hwang, J., Cho, S., Lee, G., Hwang, J., Cho, S., 2021. A novel index to detect vegetation in urban areas using UAV-based multispectral images. Appl. Sci. 11 (8). https://doi.org/10.3390/app11083472.

Lemenkova, P., Lemenkova, P., 2018. Detection of Vegetation Coverage Detection of Vegetation Coverage in Urban Agglomeration of Brussels by NDVI Indicator Using eCognition Software and Remote Sensing Measurements, 2018. https://doi.org/10.6084/m9.figshare.

Lennert, J., Farkas, J., Kovács, A.D., Molnár, A., Módos, R., Baka, D., Kovács, Z., 2020. Measuring and predicting long-term land cover changes in the functional urban area of Budapest. Sustainability 12 (8), 3331. https://doi.org/10.3390/su12083331.

Li, X., Zhang, G., Cui, H., Hou, S., Wang, S., Li, X., Chen, Y., Li, Z., 2022. MCANet: a joint semantic segmentation framework of optical and SAR images for land use classification. Int. J. Appl. Earth Obs. Geoinf. 106, 102638 https://doi.org/10.1016/j.jag.2021.102638.

Lia, Z., Zhang, H., Fangxiao, L., Xue, R., Yang, G., Zhang, L., 2022. Breaking the resolution barrier: a low-to-high network for large-scale high-resolution land-cover mapping using low-resolution labels. ISPRS J. Photogramm. Remote Sens. 192, 244–267. https://doi.org/10.1016/j.isprsjprs.2022.08.008.

Linda, A.L., Geir, H.S., 2021. The content and accuracy of the CORINE Land Cover dataset for Norway. Int. J. Appl. Earth Obs. Geoinf. 96, 102266 https://doi.org/10.1016/j.jag.2020.102266.

Lindeburg, M.R., 1999. Civil Engineering Reference Manual for the Pe Exam, 7th ed. Professional Pubns Inc., Belmont CA. 22-10ISBN-13: 978-1888577402.

Liu, A., Wu, Q., Cheng, X., 2020. Using the Google Earth Engine to estimate a 10 m resolution monthly inventory of soil fugitive dust emissions in Beijing, China. Sci. Total Environ. 735, 139174 https://doi.org/10.1016/j.scitotenv.2020.139174.

Liu, Y., Meng, Q., Zhang, L., Wu, C., 2022. NDBSI: a normalized difference bare soil index for remote sensing to improve bare soil mapping accuracy in urban and rural areas. CATENA 214, 106265. https://doi.org/10.1016/j.catena.2022.106265.

Lobell, D.B., 2013. The use of satellite data for crop yield gap analysis. Field Crop. Res. 143, 56–64. https://doi.org/10.1016/j.fcr.2012.08.008.

Lóczy, D., 1997. Human impact on rivers in Hungary as reflected in changes of channel planform. Z. Geomorphol 110, 219–231.

Lóczy, D., Éva, K., Schweitzer, F., 2009. Local flood hazards assessed from channel morphometry along the Tisza River in Hungary. Geomorphology 113 (3–4), 200–209. https://doi.org/10.1016/j.geomorph.2009.03.013.

Lu, D., Batistella, M., Moran, E., de, M.E., 2008. A comparative study of Landsat TM and SPOT HRG images for vegetation classification in the Brazilian Amazon. Photogramm. Eng. Remote Sensing. 74 (3), 311–321, 10.14358 %2Fpers.74.3.311.

Lunetta, R.S., Congalton, R.G., Fenstermaker, L.K., Jensen, J.R., McGwire, K.C., Tinney, L.R., 1991. Remote sensing and geographic information system data integration: error sources and research issues. Photogrammetr. Eng., Remote Sens. 57 (6), 677–687.

Ma, X., Xu, J., Luo, Y., Aggarwal, S.P., Li, J., 2009. Response of hydrological processes to land-cover and climate changes in Kejie watershed, south-west China. Hydrol. Process. 23 (8), 1179–1191. https://doi.org/10.1002/hyp.7233.

Malcom, H.R., 1997. Elements of Storm water Design, 85. North Carolina State University, Industrial Extension Service, Raleigh, NC. Available online. https://www.deq.nc.gov/water-quality/surface-water-protection/spu/spu-bmp-manual-documents/bmpman-appendix-b-20070629-dwq-spu/download.

Manandhar, B., Cui, S., Wang, L., Shrestha, S., 2023. Urban flood hazard assessment and management practices in South Asia: a review. MDPI Land 12 (3). https://doi.org/10.3390/land12030627.

Matsushita, B., Yang, W., Chen, J., Onda, Y., Qiu, G., 2007. Sensitivity of the enhanced vegetation index (EVI) and normalized difference vegetation index (NDVI) to topographic effects: a case study in high-density cypress forest. Sens. (Basel) 7 (11), 2636–2651, 10.3390%2Fs7112636.

Matthews, F., Verstraeten, G., Borrelli, P., Panagos, P., 2022. A field parcel-oriented approach to evaluate the crop cover-management factor and time-distributed erosion risk in Europe. Int. Soil Water Conserv. Res. 11 (1), 43–59. https://doi.org/10.1016/j.iswcr.2022.09.005.

Medina, J.A.V., Beatriz, E.A.A., 2018. Comparison of maximum likelihood, support vector machines, and random forest techniques in satellite images classification. Tecnura 23 (59), 13–26. https://doi.org/10.14483/22487638.14826.

Mehmood, M., Shahzad, A., Zafar, B., Shabbir, A., Ali, N., 2022. Remote Sensing Image Classification: A Comprehensive Review and Applications. Mathematical Problems in Engineering. Application of Machine Learning in Civil Engineering. https://doi.org/10.1155/2022/5880959.

Michelle, T.H.V., Edward, R.J., Martina, F., Wietse, H.P.F., Naota, H., Yoshihide, W., John, R.Y., 2021. Global water scarcity including surface water quality and expansions of clean water technologies. Environ. Res. Lett. 16, 024020 https://doi.org/10.1088/1748-9326/abbfc3.

Milly, P.C.D., Betancourt, J., Falkenmark, M., Hirsch, R.M., Kundzewicz, Z.W., Lettenmaier, D.P., Stouffer, R.J., 2008. Stationarity is dead: whither water management? Science 319 (5863), 573–574. https://doi.org/10.1126/science.1151915.

Mobilian, C., Craft, C.B., 2022. Wetland Soils: Physical and Chemical Properties and Biogeochemical Processes, 2nd Edition, 3. Encyclopedia of Inland Waters, pp. 157–168. https://doi.org/10.1016/B978-0-12-819166-8.00049-9.

Molnár, E., Dézsi, G., Lengyel, I.M., Kozma, G., 2018. Vidéki nagyvárosaink gazdaságának összehasonlító elemzése (A comparative analysis of the Hungarian minor cities). Területi. Stat. 58, 610–637. https://doi.org/10.15196/TS580604.

Molnár, E., Kozma, G., 2018. A debreceni gazdaságfejlesztés zászlóshajói: a városban működő ipari parkok jellegzetességei. (Flagships of economic development of Debrecen: characteristics of industrial parks in the city). Tér és Társadalom 33 (3), 49–71. https://doi.org/10.17649/TET.33.3.3188.

Mondejar, J.P., Alejandro, F.T., 2019. Near infrared band of Landsat 8 as water index: a case study around Cordova and Lapu-Lapu City, Cebu, Philippines. Sustain. Environ. Res. 29 (16) https://doi.org/10.1186/s42834-019-0016-5.

Monaghan, R.M., Laurenson, S., Dalley, D.E., Orchiston, T.S., 2017. Grazing strategies for reducing contaminant losses to water from forage crop fields grazed by cattle during winter. N. Zeal. J. Agric. Res. 60 (3), 333–348. https://doi.org/10.1080/00288233.2017.1345763.

Moradi, M., Scott, E., Amir, K., 2022. A Comprehensive Indoor–Outdoor Urban Climate Model With hydrology: The Vertical City Weather Generator (VCWG v2.0.0), 207. Building and Environment, 108406. https://doi.org/10.1016/j.buildenv.2021.108406.

Morton, F.I., 1986. Practical estimates of lake evaporation. J. Appl. Meteorol. Climatol 25 (3), 371–387, 10.1175/1520-0450(1986)025%3C0371:PEOLE%3E2.0.CO;2.

Mtibaa, S., Asano, S., 2022. Hydrological evaluation of radar and satellite gauge-merged precipitation datasets using the SWAT model: case of the Terauchi catchment in Japan. J. Hydrol. Reg. Stud. 42, 101134 https://doi.org/10.1016/j.ejrh.2022.101134.

Mustapha, M.R., Lim, H.S., Mat Jafri, M.Z., 2010. Comparison of neural network and maximum likelihood approaches in image classification. Journal of Applied Sciences 10 (22), 2847–2854. https://doi.org/10.3923/jas.2010.2847.2854.

Musy, A., Higy, C., 2004. Hydrologie, Une Science De La Nature. Presses Polytechniques et Universitaires Romandes, French, p. 314 pISBN: 9782880745462.

Naboureh, A., Bian, J., Lei, G., Li, A., 2020. A review of land use/land cover change mapping in the China-Central Asia-West Asia economic corridor countries. Big Earth Data 5 (2). https://doi.org/10.1080/20964471.2020.1842305.

Naesset, E., 1996. Conditional tau coefficient for assessment of producer's accuracy of classified remotely sensed data. ISPRS J. Photogramm. Remote Sens. 51 (2), 91–98. https://doi.org/10.1016/0924-2716(69)00007-4.

[Nagy, A., Tamás, J., 2009. Integrated airborne and field methods to characterize soil water regime. In: Celkova, A. (Ed.), Proceedings of peer-reviewed contributions, Transport of water, chemicals, and energy in the soil-plant-atmosphere system. Bratislava. Institute of Hydrology, Slovak Academy of Sciences, pp. 412–420.].

Nagy, A., Tamás, J., 2013. Noninvasive water stress assessment methods in orchards. Commun. Soil Sci. Plant Anal. 44, 366–376. https://doi.org/10.1080/00103624.2013.742308, 1-4.

Nagy, A., Tamás, J., Burai, P., 2007. Application of advanced technologies for the detection of pollution migration. Cereal Res. Commun. 35, 805–809. Available online. https://www.researchgate.net/publication/250010299_Application_of_advanced_technologies_for_the_detection_of_pollution_migration.

Nguyen, K.D., Tadashi, S., 2012. The responses of hydrological processes and sediment yield to land-use and climate change in the Be River Catchment, Vietnam. Hydrol. Process. 28 (3), 640–652. https://doi.org/10.1002/hyp.9620.

Nieuwenhuis, E., Cuppen, E., Langeveld, J., Bruijn, H., 2021. Towards the integrated management of urban water systems: conceptualizing integration and its uncertainties. J. Clean. Prod. 280, 124977 https://doi.org/10.1016/j.jclepro.2020.124977.

Njoku, E.A., Tenenbaum, D.E., 2022. Quantitative assessment of the relationship between land use/land cover (LULC), topographic elevation and land surface temperature (LST) in Ilorin, Nigeria. Remote Sens. Appl.: Soc. Environ. 27, 100780 https://doi.org/10.1016/j.rsase.2022.100780.

Nwagoum, C.S.K., Yemefack, M., Tedou, F.B.S., Oben, F.T., 2023. Sentinel-2 and Landsat-8 potentials for high-resolution mapping of the shifting agricultural landscape mosaic systems of southern Cameroon. Int. J. Appl. Earth Obs. Geoinf. 124 https://doi.org/10.1016/j.jag.2023.103545.

Office cantonal de l'eau (OCEau), 2005. Méthode simplifiée pour le dimensionnement et la conception des ouvrages de rétention pour les petits bassins versants urbanisés. Gestion Quantitative Des Eaux Pluviales. Genève, un canton d'eau. Département du territoire (DT) (République et canton de Genève), p. 25. Version 1.1p.

Osorio, J., Jeong, J., Bieger, K., Arnold, J., 2014. Influence of Potential Evapotranspiration on the Water Balance of Sugarcane Fields in Maui, Hawaii. J. Water Resour. Prot. 6 (9) https://doi.org/10.4236/jwarp.2014.69080.

Padma, S., Sanjeevi, S., 2014. Jeffries Matusita based mixed-measure for improved spectral matching in hyperspectral image analysis. Int. J. Appl. Earth Obs. Geoinf. 32, 138–151. https://doi.org/10.1016/j.jag.2014.04.001.

Pásztor, L., Laborczi, A., Bakacsi, Z., Szabó, J., Illés, G., 2018. Compilation of a national soil-type map for Hungary by sequential classification methods. Geoderma 311, 93–108. https://doi.org/10.1016/j.geoderma.2017.04.018.

Pénzes, J., Hegedűs, L.D., Makhanov, K., Túri, Z., 2023. Changes in the patterns of population distribution and built-up areas of the rural–urban fringe in post-socialist context—a Central European case study. Land (Basel) 12, 1682. https://doi.org/10.3390/land12091682.

Poleman, H., 2018. Assessing Access to Green Areas in Europe's Cities. Update Using Completed Copernicus Urban Atlas Data. In A Walk to the Park? Assessing Access to Green Areas in Europe's Cities. European Commission.; DG for Regional and Urban Policy. Dijkstra, Lp16. Available online. https://ec.europa.eu/regional_policy/en/information/publications/working-papers/2018/a-walk-to-the-park-assessing-access-to-green-areas-in-europe-s-cities.

Pontius Jr, R.G.J., 2000. Quantification error versus location in comparison of categorical maps. Photogramm. Eng. Remote Sens. 66 (8), 1011–1016. Available online. https://www.asprs.org/wp-content/uploads/pers/2000journal/august/2000_aug_1011-1016.pdf.

Pontius Jr, R.G., 2022. Metrics That Make a Difference. Switzerland. ISBN-10: 3030707644.

Pontius Jr, R.G., Millones, M, 2011. Death to kappa: birth of quantity disagreement and allocation disagreement for accuracy assessment. Int. J. Remote Sens. 32 (15), 4407–4429. https://doi.org/10.1080/01431161.2011.552923.

Pontius Jr, R.G., Millones, M., 2008. Problems and solutions for kappa-based indices of agreement. In: Paper presented at the International Conference on Studying, Modeling and Sense Making of Planet Earth. Mytilene, Greece. June 1–6.

Pregun, C.Z., 2022. Dynamics of self-regulatory processes in a lowland river due to seasonal changes in certain hydro-ecological and water quality factors. Ecol. Eng. 178, 106595 https://doi.org/10.1016/j.ecoleng.2022.106595.

Qin, Q., Xu, D., Hou, L., Shen, B., Xin, X., 2021. Comparing vegetation indices from Sentinel-2 and Landsat 8 under different vegetation gradients based on a controlled grazing experiment. Ecol. Indic. 133, 108363 https://doi.org/10.1016/j.ecolind.2021.108363.

Qingyan, S., Chuiyu, L., Hui, G., Lingjia, Y., Xin, H., Tao, Q., Chu, W., Qinghua, L., Bo, Z., Zepeng, L., 2021. Study on hydrologic effects of land use change using a distributed hydrologic model. Water MDPI 13 (4), 447.604. https://doi.org/10.3390/w13040447.

Qiu, G.Y., Zou, Z., Li, X., Li, H., Guo, Q., Yan, C., Tan, S., 2017. Experimental studies on the effects of green space and evapotranspiration on urban heat island in a subtropical megacity in China. Habitat Int. 68, 30–42. https://doi.org/10.1016/j.habitatint.2017.07.009.

Roy, D.P., Kovalskyy, V., Zhang, H.K., Vermote, E.F., Yan, L., Kumar, S.S., Egorov, A., Roy, D.P., Kovalskyy, V., Zhang, H.K., Vermote, E.F., Yan, L., Kumar, S.S., Egorov, A., 2016a. Characterization of Landsat-7 to Landsat-8 reflective wavelength and normalized difference vegetation index continuity. Remote Sens. Environ. 185, 57–70. https://doi.org/10.1016/j.rse.2015.12.024.

Roy, D.P., Wulder, M.A., Loveland, T.R., Woodcock, C.E., 2014. Landsat-8: science and product vision for terrestrial global change research. Remote Sens. Environ. 145, 154–172. https://doi.org/10.1016/j.rse.2014.02.001.

Rahman, Z.A., Al Kafy, A., Saha, M., Rahim, A.A., Almulhim, A.I., Rahman, S.N., Fattah, M.A., Rahman, M.T., Kalaivani, S., Faisal, A.A., Rakib, A.A., 2022. Assessing the impacts of vegetation cover loss on surface temperature, urban heat island and carbon emission in Penang city, Malaysia. Build Environ. 222, 109335 https://doi.org/10.1016/j.buildenv.2022.109335.

Tamás, J., Nagy, A., Buday-Bódi, E., Gálya, B., Nistor, S., Fehér, J., 2019. Guideline - Application of the Process Oriented Spatial Decision Support Tools: Methods in Urban Hydrology For Middle-Sized Cities in CEE Based on the Reference Sites. University of Debrecen. Debrecen 93. ISBN: 978-963-490-162-4.

Ramier, D., Berthier, E., Andrieu, H., 2011. The hydrological behavior of urban streets: long-term observations and modelling of runoff losses and rainfall–runoff transformation. Hydrol. Process. 25 (14), 2161–2178. https://doi.org/10.1002/hyp.7968.

Rembold, F., Atzberger, C., Rojas, O., Savin, I., 2013. Using low resolution satellite imagery for yield prediction and yield anomaly detection. MDPI Remote Sens. 5 (11), 5572–5573. https://doi.org/10.3390/rs5041704.

Rong, C., Fu, W., 2023Rong, C., Fu, W., 2023. A comprehensive review of land use and land cover change based on knowledge graph and bibliometric analyses. Land 12 (8), 1573. https://doi.org/10.3390/land12081573.

Rosenfield, G.H., Fitzpatrick, L.K., 1986. A coefficient of agreement as a measure of thematic classification accuracy. Photogram. Eng. Remote Sens. 52, 223–227. Avalable online. https://www.asprs.org/wp-content/uploads/pers/1986journal/feb/1986_feb_223-227.pdf. Available online:

Safari, F., De Smedt, F., Moreda, F., 2012. WetSpa model application in the Distributed Model Intercomparison Project (DMIP2). J. Hydrol. 418–419, 78–89. https://doi.org/10.1016/j.jhydrol.2009.04.001.

Sajikumar, N., Remya, R.S., 2015. Impact of land cover and land use change on runoff characteristics. J. Environ. Manage. 161, 460–468. https://doi.org/10.1016/j.jenvman.2014.12.041.

Sajjad, H., Mubeen, M., Karuppannan, S., 2022. Land use and land cover (LULC) change analysis using TM, ETM+ and OLI Landsat images in district of Okara, Punjab, Pakistan. Phys. Chem. Earth. Parts A/B/C. 126, 103117 https://doi.org/10.1016/j.pce.2022.103117.

Sampaio, G., Nobre, C., Costa, M.H., Satyamurty, P., Soares-Filho, B.S., Cardoso, M., 2007. Regional climate change over eastern Amazonia caused by pasture and soybean cropland expansion. Geophys. Res. Lett. 34 (17) https://doi.org/10.1029/2007GL030612.

Sandu, M.A., Virsta, A., 2015. Applicability of MIKE SHE to simulate hydrology in argesel river catchment. Agricult. Agricult. Sci. Procedia 6, 517–524. https://doi.org/10.1016/j.aaspro.2015.08.135.

Schoenbaum, I., Henkin, Z., Yehuda, Y., Voet, H., Kigel, J., 2018. Cattle foraging in Mediterranean oak woodlands effects of management practices on the woody vegetation. For. Ecol. Manage. 419–420, 160–169. https://doi.org/10.1016/j.foreco.2018.03.017.

Schott, J.R., 2002. Remote Sensing: Active and Passive Systems and Applications, 1st ed. Oxford University Press. Chapter 13: Image Classification.

Seto, K.C., Fragkias, M., Güneralp, B., Reilly, M.K., 2011. A meta-analysis of global urban land expansion. PLoS ONE 6 (8). https://doi.org/10.1371/journal.pone.0023777.

Shi, D., Yang, X., 2015. Support Vector Machines For Land Cover Mapping from Remote Sensor Imagery. Monitoring and Modeling of Global Changes: A Geomatics Perspective. Springer Remote Sensing/Photogrammetry, pp. 265–279. https://doi.org/10.1007/978-94-017-9813-6_13.

Smerdon, B.D., Allen, D.M., Grasby, S.E., Berg, M.A., 2009. An approach for predicting groundwater recharge in mountainous watersheds. J. Hydrol. 365 (3–4), 156–172. https://doi.org/10.1016/j.jhydrol.2008.11.023.

Soil and Water Conservation Society, 2003. Conservation Implications of Climate change: Soil erosion and Runoff from Cropland. SWCS Rep, p. 24 pp. https://www.swcs.org/static/media/cms/Climate_changefinal_112904154622.pdf.

Somlyai, I., Berta, C., Nagy, S.A., Dévai, G., Ács, É., Szabó, L.J., Nagy, J., Grigorszky, I., 2019. Heterogeneity and Anthropogenic Impacts on a Small Lowland Stream. Water. 11 (10) https://doi.org/10.3390/w11102002.

Son, J., Kwon, T., 2022. Evaluation and improvement measures of the runoff coefficient of urban parks for sustainable water balance. Land. 11 (7), 1098. https://doi.org/10.3390/land11071098.

Srivastav, A.L., Madhav, S., Bhardwaj, A.K., Jones, E.V., 2022. Urban water crisis and management: strategies for sustainable development. Curr. Direct. Water Scarc. Res. 6. ISBN: 9780323918381.

Su, M., Guo, R., Chen, B., Hong, W., Wang, J., Feng, Y., Xu, B., 2020. Sampling strategy for detailed urban land use classification: a systematic analysis in Shenzhen. Remote Sens. 12 (9), 1497. https://doi.org/10.3390/rs12091497.

Szalai, S., Bihari, Z., Lakatos, M., Szentimrey, S., 2005. Some characteristics of Hungary's climate from 1901 to the present day. Natl. Meteorolog. Serv.

Szász, G., 2013. Agrometeorological research and its results in Hungary (1870–2010). Q. J. Hungar. Meteorolog. Serv. 117 (3), 315–358.

Szilassi, P., 2017. Magyarországi kistájak felszínborítás változékonysága és felszínborítás mozaikosságuk változása. Tájökológiai Lapok 15 (2), 131–138. https://doi.org/10.56617/tl.3612.

Talha, M., Farrukh, A.B., Sajid, G., Hamza, Z., 2023. ADU-Net: semantic segmentation of satellite imagery for land cover classification. Adv. Space Res. 72 (5), 1780–1788. https://doi.org/10.1016/j.asr.2023.05.007.

Tallis, H.T., Ricketts, T., Guerry, A.D., Wood, S.A., Sharp, R., Nelson, E., Ennaanay, D., Wolny, S., Olwero, N., Vigerstol, K., Pennington, D., Mendoza, G., Aukema, J., Foster, J., Cameron, D., Arkema, K., Lonsdorf, E., Kennedy, C., Verutes, G., Kim, C.K., Guannel, G., Papenfus, M., Toft, J., Marsik, M., Bernhardt, J., Griffin, R., Glowinski, K., Chaumont, N., Perelman, A., Lacayo, M., 2013. A Modeling Suite Developed By The Natural Capital Project to Support Environmental Decision Making 347.

Talukdar, S., Singha, P., Mahato, S., Shahfahad, Pal, S., Liou, Y.A., Rahman, A., 2020. Land-use land-cover classification by machine learning classifiers for satellite observations a review. Remote Sens. 12 (7), 1135. https://doi.org/10.3390/rs12071135.

Tarawally, M., Wenbo, X., Weiming, H., Mushore, T.D., Kursah, M.B., 2019. Land use/land cover change evaluation using land change modeller: a comparative analysis between two main cities in Sierra Leone. Remote Sens. Appl.: Soc. Environ. 16, 100262 https://doi.org/10.1016/j.rsase.2019.100262.

The Comet ® Program, 2010. Runoff Processes: International Edition. University Corporation for Atmospheric Research. Available online. https://www.meted.ucar.edu/hydro/basic_int/runoff/navmenu.php.

Thorndahl, S., Nielsen, J.E., Rasmussen, M.R., 2019. Estimation of storm-centred areal reduction factors from radar rainfall for design in urban hydrology. Water (Basel) 11 (6), 1120. https://doi.org/10.3390/w11061120.

Tony, V.M.S., Jorge, R., 2022. On the quality of the drainage network cartographic representation. Ecol. Indic. 143, 109350 https://doi.org/10.1016/j.ecolind.2022.109350.

Town of Buckeye Public Works Department, 2007. Storm Water Drainage System Design Manual 70 p.

Tucker, C.J., 1979. Red and photographic infrared linear combinations for monitoring vegetation. Remote Sens. Environ. 8 (2), 127–150. https://doi.org/10.1016/0034-4257(79)90013-0.

Turc, L., 1961. Water requirements assessment of irrigation, potential evapotranspiration: simplified and updated climatic formula. Annales Agronomiques 12, 13–49.

UNESCO OMM AISH, 1974. Design of Water Resources Projects With Inadequate data: Proceedings of the Madrid Symposium, 1. Élaboration des projets d'utilisation des ressources en eau sans données suffisantes: actes du Colloque de Madrid. VolISBN: 92-3-001137-1. https://unesdoc.unesco.org/ark:/48223/pf0000013828.

Urbancsek, J., 1960. Az alföldi artézi kutak fajlagos vízhozama és abból levonható vízföldtani és ősföldrajzi következtetések. Hidrol. Közl. 40 (5), 398–403.

USGS, 2016. Earth explorer. URL: https://earthexplorer.usgs.gov/.

Várallyay, G.Y., Molnár, S., 1989. The agro-topographical map of Hungary. Hungarian Cartographical Studies. In: 14th World Conf. ICA-ACI. Budapest, pp. 221–225.

Varga, O.G., Pontius Jr, R.G., Singh, S.K., Szabó, S., 2019. Intensity analysis and the Figure of Merit's components for assessment of a cellular automata–Markov

simulation model. Ecol Indic 101, 933–942. https://doi.org/10.1016/j.ecolind.2019.01.057.

Vrebos, D., Vansteenkiste, T., States, J., Willems, P., Meire, P., 2014. Water displacement by sewer infrastructure in the Grote Nete catchment, Belgium, and its hydrological regime effects. Hydrol. Earth Syst. Sci. 18, 1119–1136. https://doi.org/10.5194/hessd-10-7425-2013.

Weng, Q., Lu, D., 2008. A sub-pixel analysis of urbanization effect on land surface temperature and its interplay with impervious surface and vegetation coverage in Indianapolis, United States. Int. J. Appl. Earth Obs. Geoinf. 10 (1), 68–83. https://doi.org/10.1016/j.jag.2007.05.002.

Williams, P., Whitfield, M., Biggs, J., Bray, S., Fox, G., Nicolet, P., Sear, D., 2004. Comparative biodiversity of rivers, streams, ditches and ponds in an agricultural landscape in Southern England. Biol. Conserv. 115 (2), 329–341. https://doi.org/10.1016/S0006-3207(03)00153-8.

Xu, X., Long, D., Li, X., Wang, Y., Zhao, F., Cui, Y., 2024. Unveiling Lake Ice Phenology in Central Asia Under Climate Change with MODIS Data and a Two-Step Classification Approach, 301. https://doi.org/10.1016/j.rse.2023.113955.

Yang, J., Xu, C., Ni, X., Zhang, X., 2022. Study on urban rainfall–runoff model under the background of inter-basin water transfer. Water. 14 (17), 2660. https://doi.org/10.3390/w14172660.

Yonaba, R., Koïta, M., Mounirou, L.A., Tazen, F., Queloz, P., Biaou, A.C., Niang, D., Zouré, C., Karambiri, H., Yacouba, H., 2021. Spatial and transient modelling of land use/land cover (LULC) dynamics in a Sahelian landscape under semi-arid climate in northern Burkina Faso. Land Use Policy 103, 105305. https://doi.org/10.1016/j.landusepol.2021.105305.

Zhou, G.Y., Morris, J.D., Yan, J.H., Yu, Z.Y., Peng, S.L., 2002. Hydrological impacts of reforestation with eucalypts and indigenous species: a case study in southern China. For. Ecol. Manag. 167 (1–3), 209–222. https://doi.org/10.1016/S0378-1127(01)00694-6.

Zhou, Q., Tollerud, H., Barber, C., Smith, K., Zelenak, D., 2022. Training data selection for annual land cover classification for the land change monitoring, assessment, and projection (LCMAP) initiative. Remote Sens. 12 (4), 699. https://doi.org/10.3390/rs12040699.

Zhu, Z., Gallant, A.L., Woodcock, C.E., Pengra, B., Olofsson, P., Loveland, T.R., Jin, S., Dahal, D., Yang, L., Auch, R.F., 2016. Optimizing selection of training and auxiliary data for operational land cover classification for the LCMAP initiative. ISPRS J. Photogramm. Remote Sens. 122, 206–221. https://doi.org/10.1016/j.isprsjprs.2016.11.004.